

Supplementary Material

Cyanine–cyanine hybrid structure as a stabilized polyelectrochromic system: synthesis, stabilities, and redox behavior of di(1-azulenyl)methylium units connected with electron-accepting π -electron systems

Shunji Ito,^{*,†} Ryuta Sekiguchi,[‡] Akira Mizushima,[†] Kohei Kudo,[†] Jun Kawakami,[†] and Taku Shoji[‡]

[†] Graduate School of Science and Technology, Hirosaki University, Hirosaki 036-8561, Aomori, Japan

[‡] Department of Chemistry, Faculty School of Science, Shinshu University, Matsumoto 390-8621, Nagano, Japan

Email: itsnj@hirosaki-u.ac.jp

Table of Contents

1. Experimental details for physical measurements	S2
2. pK_R^+ data of 5a ⁺ , 5b ⁺ , 8a ⁺ , 8b ⁺ , 11a–d ⁺ , and 14 ⁺	S3
3. CV and DPV waves of 5a ⁺ , 5b ⁺ , 8a ⁺ , 8b ⁺ , 11a–d ⁺ , and 14 ⁺	S13
4. Spectroelectrograms of 5a ⁺ , 5b ⁺ , 8a ⁺ , 8b ⁺ , 11a–d ⁺ , and 14 ⁺	S33
5. Copies of ¹ H and ¹³ C NMR spectra of reported compounds	S42

1. Experimental details for physical measurements

pK_R^+ Value Measurements: Sample solutions of the hexafluorophosphates $5a^+PF_6^-$, $8a^+PF_6^-$, $11a-d^+PF_6^-$, and $14^+PF_6^-$ were prepared by dissolving 1–2 mg of the hexafluorophosphates in MeCN and a glycine (0.1 M) solution (50 mL) and made up to 100 mL by further adding MeCN; the sample solution with lower acidity was made by further alkalification with 20% aqueous NaOH. For the preparation of a sample solution of the hexafluorophosphates $5b^+PF_6^-$ and $8b^+PF_6^-$, buffer solutions of slightly different acidities were prepared by mixing CH_3COONa (1 M) and HCl (1 M) for pH 1.0–3.0, CH_3COONa (0.1 M) and CH_3COOH (0.1 M) for pH 3.2–5.0, KH_2PO_4 (0.1 M) and $Na_2B_4O_7$ (0.05 M) for pH 6.0–9.0, $Na_2B_4O_7$ (0.05 M) and Na_2CO_3 (0.05 M) for pH 10.0, and $Na_2B_4O_7$ (0.05 M) and $NaOH$ (0.1 M) for pH 11.0–11.4, in various portions. Each 1 mL portion of the stock solution, prepared by dissolving 2–3 mg of the hexafluorophosphates $5b^+PF_6^-$ and $8b^+PF_6^-$ in MeCN (20 mL), was pipetted out and made up to 10 mL by adding an appropriate buffer solution (5 mL) and MeCN. The pH of each sample was made on a Horiba pH meter F-13 calibrated with standard buffers before use. The observed absorbance at the specific absorption maxima in visible region of the cations $5a^+$, $5b^+$, $8a^+$, $8b^+$, $11a-d^+$, and 14^+ were plotted against the pH, giving classical titration curves whose midpoints were taken as the pK_R^+ values.

Voltammetry Measurements: The voltammetry measurements were carried out on a ALS 610B electrochemical analyzer in benzonitrile containing Et_4NClO_4 (0.1 M) as a supporting electrolyte utilizing Pt working and auxiliary electrodes, and a reference electrode formed from $Ag/AgNO_3$ (0.01 M) in acetonitrile containing $n-Bu_4NClO_4$ (0.1 M) at the scan rate of 100 mV s^{-1} . The internal reference Fc/Fc^+ discharges at +0.15 V under these conditions.

Spectroelectrogram Measurements: Sample solutions were prepared by dissolving $5a^+PF_6^-$, $5b^+PF_6^-$, $8a^+PF_6^-$, $8b^+PF_6^-$, $11a-d^+PF_6^-$, and $14^+PF_6^-$ in benzonitrile containing Et_4NClO_4 (0.1 M) and were degassed through an Ar stream. Spectroelectrogram measurements were carried out using a quartz cell ($1 \times 10 \times 35\text{ mm}$) equipped with a Pt mesh and a wire as the working and counter electrodes, respectively, which were separated by a glass filter. A constant-current reduction and oxidation were applied to the sample solution. The electrical current was monitored by a microampere meter. The potential values are automatically increased by the resistance of the sample solution from 0 V up to $\pm 12\text{ V}$ by our constant current apparatus. Spectroelectrograms were measured on an Ocean Optics USB2000 spectrophotometer.

2. pK_a^+ data of $5a^+$, $5b^+$, $8a^+$, $8b^+$, $11a-d^+$, and 14^+ **Table S1.** pK_R^+ Values^a of $5a^+$, $5b^+$, $8a^+$, $8b^+$, $11a-d^+$, and 14^+

Sample	pK_R^{+b}	Sample	pK_R^{+b}
5a⁺	9.5 ± 0.1 (1%)	11a⁺	12.1 ± 0.1 (5%)
5b⁺	1.4 ± 0.1 (89%)	11b⁺	5.3 ± 0.1 (60%)
8a⁺	10.9 ± 0.1 (3%)	11c⁺	11.7 ± 0.1 (5%)
8b⁺	2.9 ± 0.1 (83%)	11d⁺	8.7 ± 0.1 (1%)
		14⁺	9.3 ± 0.1 (10%)

^a The pK_R^+ values were determined spectrophotometrically in a buffered solution prepared in 50% aqueous acetonitrile. ^b Regenerated absorption maxima (%) of the cations in visible region by acidification of the alkaline solution with HCl are shown in parentheses.

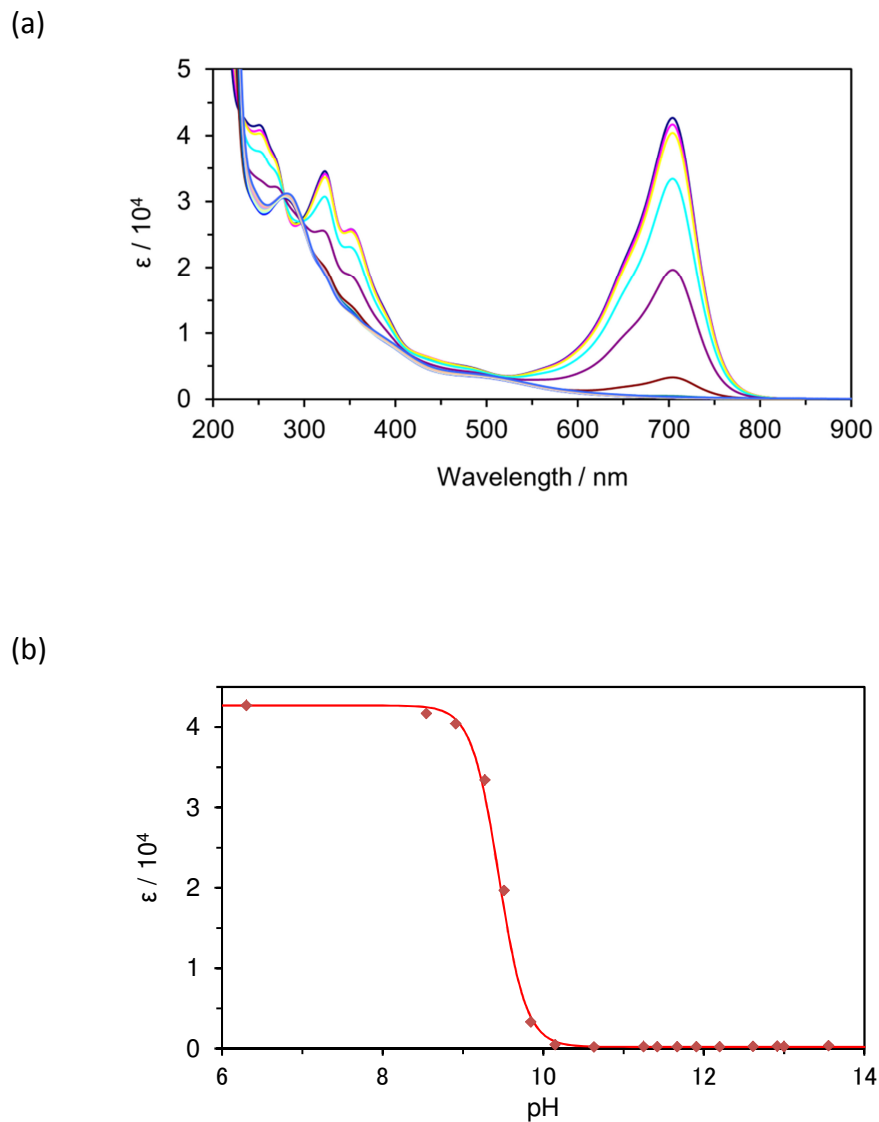


Figure S1. Continuous change in UV/Vis spectra of $5a^+$: (a) change in UV/Vis spectra and (b) a plot of pH vs. absorbance at the longest wavelength absorption maximum in base titration in 50% water/acetonitrile solution.

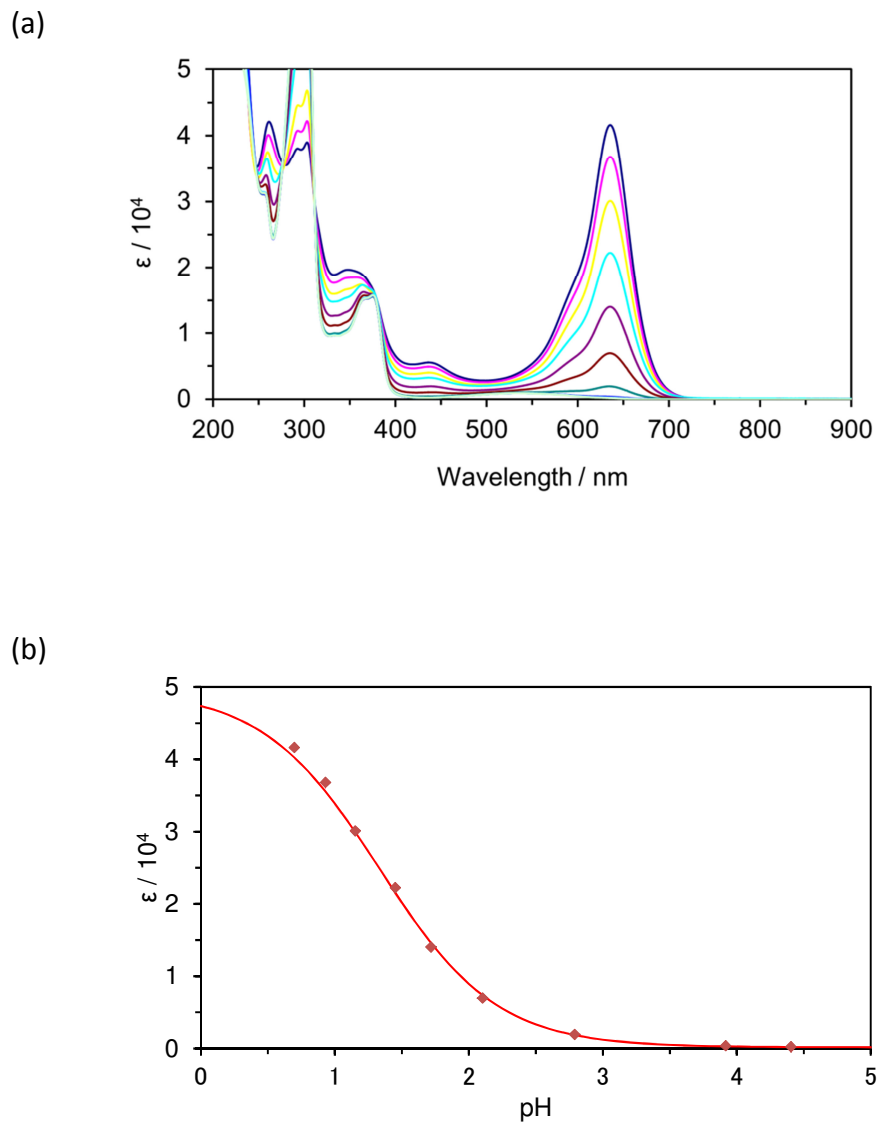


Figure S2. Continuous change in UV/Vis spectra of $5b^+$: (a) change in UV/Vis spectra and (b) a plot of pH vs. absorbance at the longest wavelength absorption maximum in base titration in 50% water/acetonitrile solution.

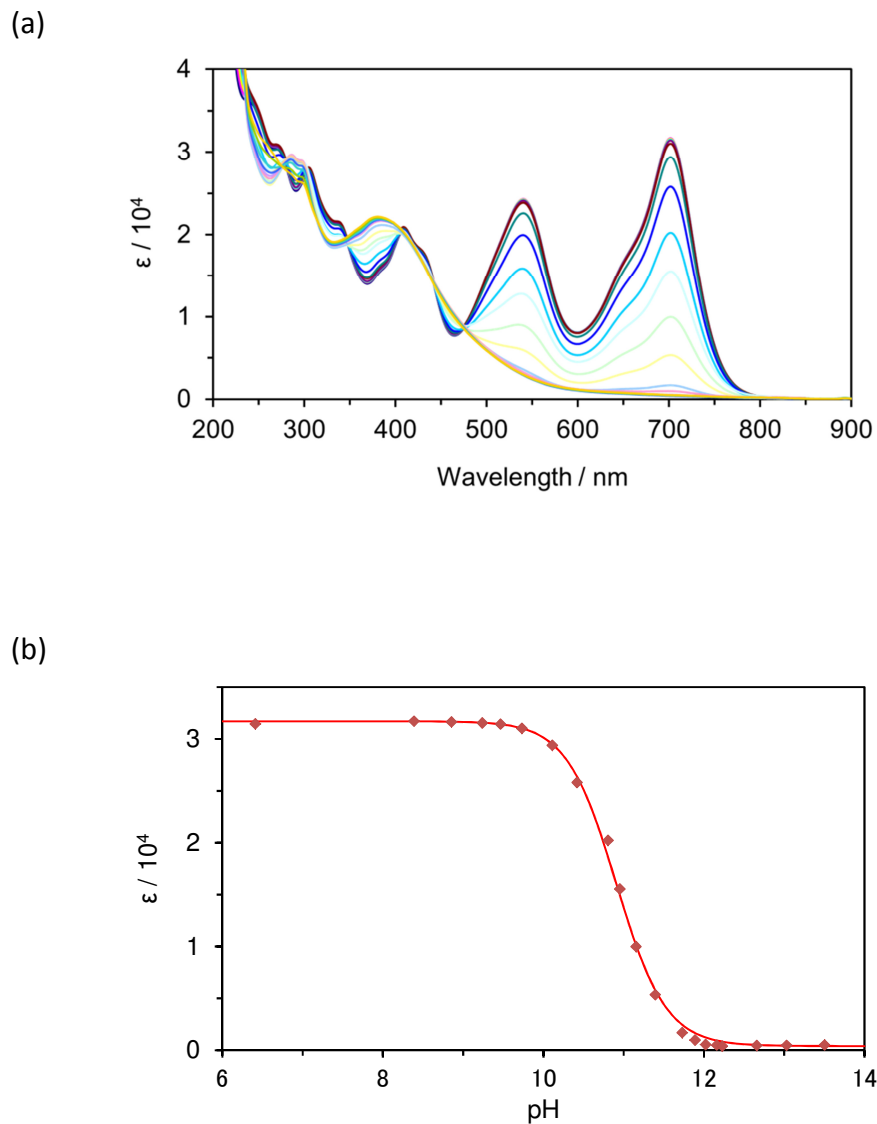


Figure S3. Continuous change in UV/Vis spectra of **8a⁺**: (a) change in UV/Vis spectra and (b) a plot of pH vs. absorbance at the longest wavelength absorption maximum in base titration in 50% water/acetonitrile solution.

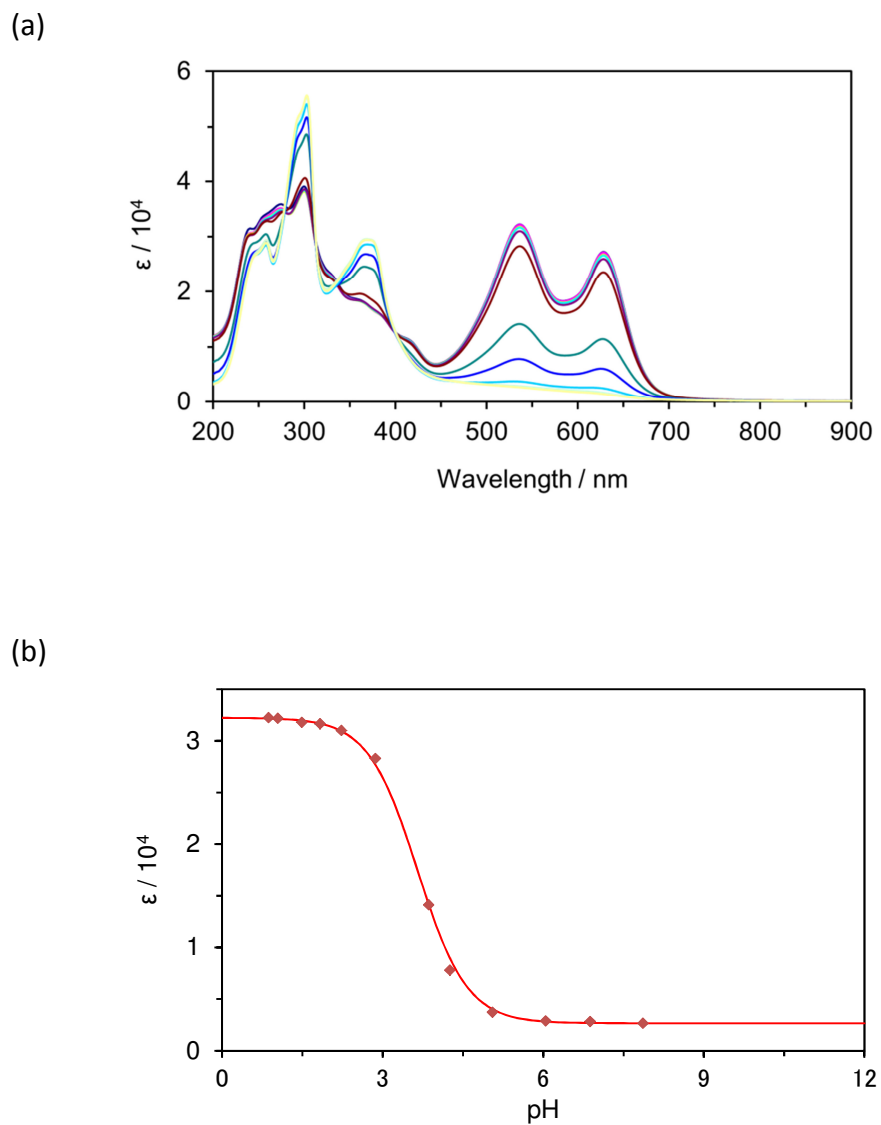


Figure S4. Continuous change in UV/Vis spectra of $8b^+$: (a) change in UV/Vis spectra and (b) a plot of pH vs. absorbance at the longest wavelength absorption maximum in base titration in 50% water/acetonitrile solution.

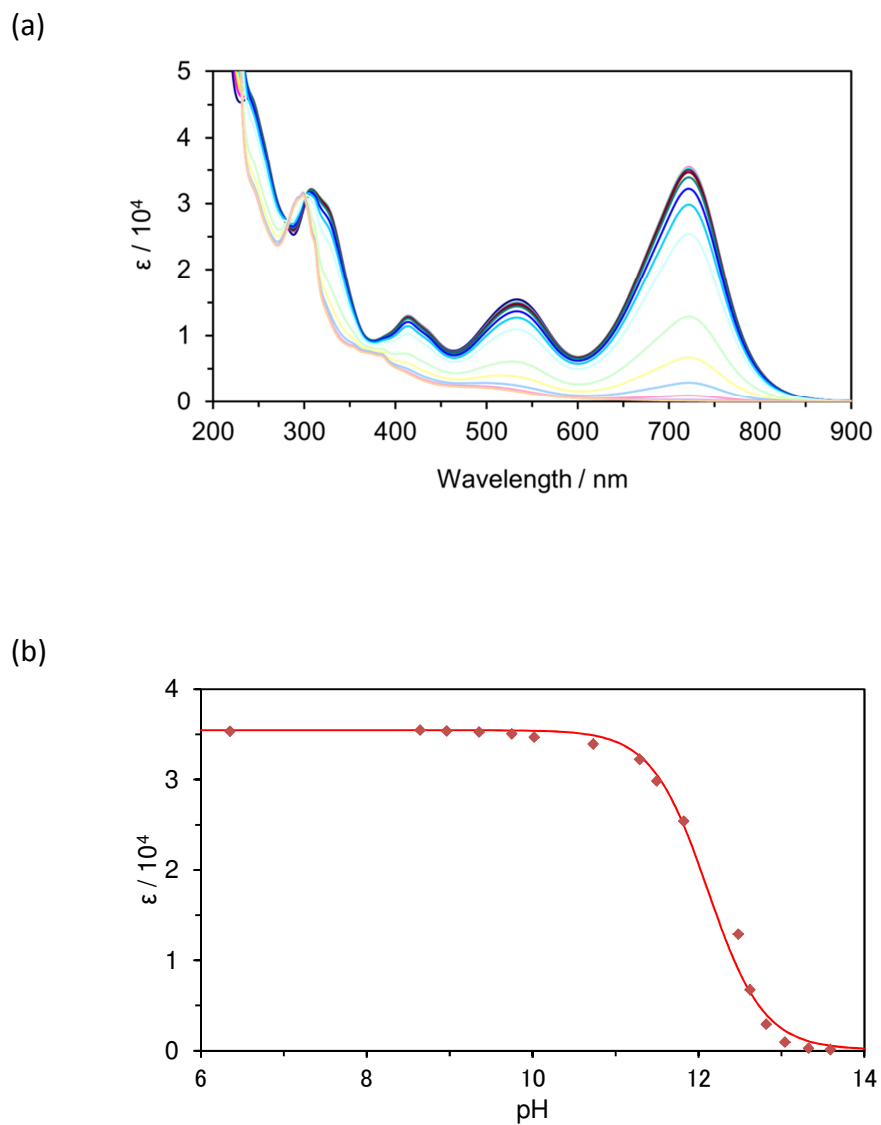


Figure S5. Continuous change in UV/Vis spectra of **11a**⁺: (a) change in UV/Vis spectra and (b) a plot of pH vs. absorbance at the longest wavelength absorption maximum in base titration in 50% water/acetonitrile solution.

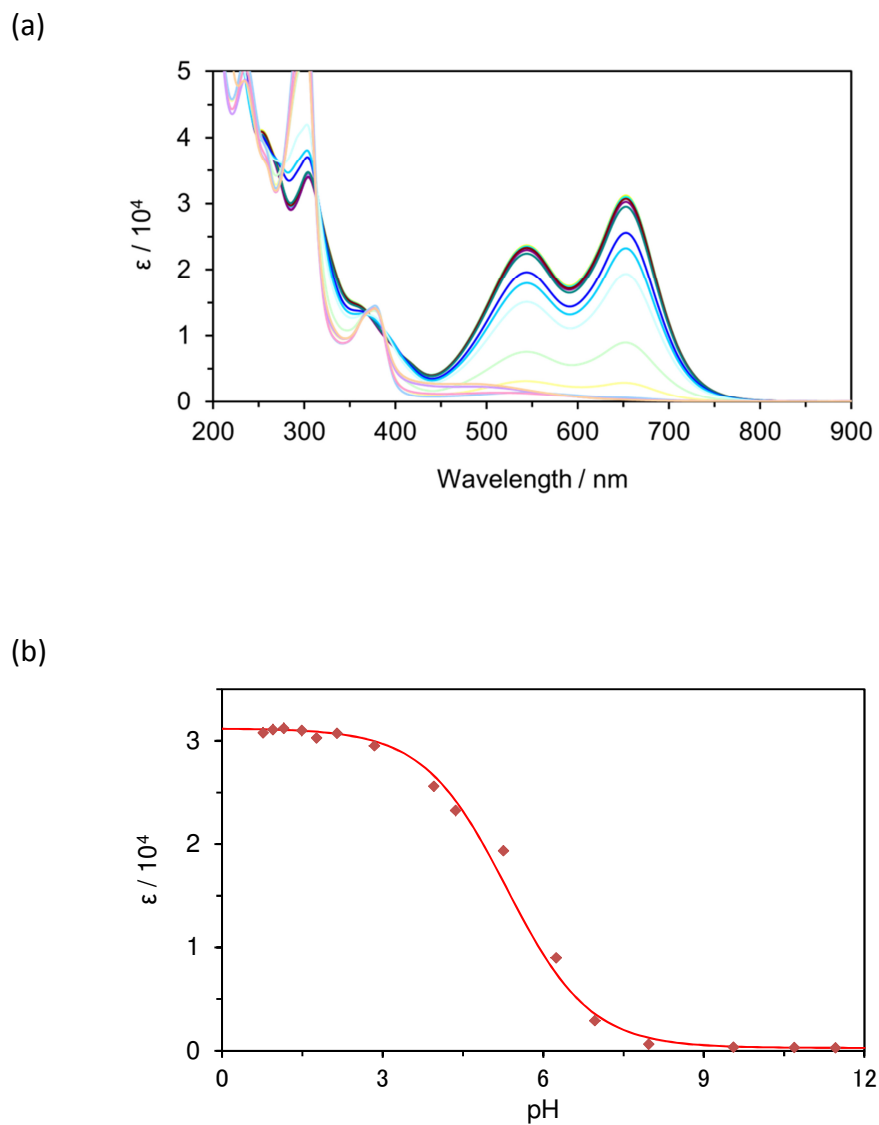


Figure S6. Continuous change in UV/Vis spectra of **11b**⁺: (a) change in UV/Vis spectra and (b) a plot of pH vs. absorbance at the longest wavelength absorption maximum in base titration in 50% water/acetonitrile solution.

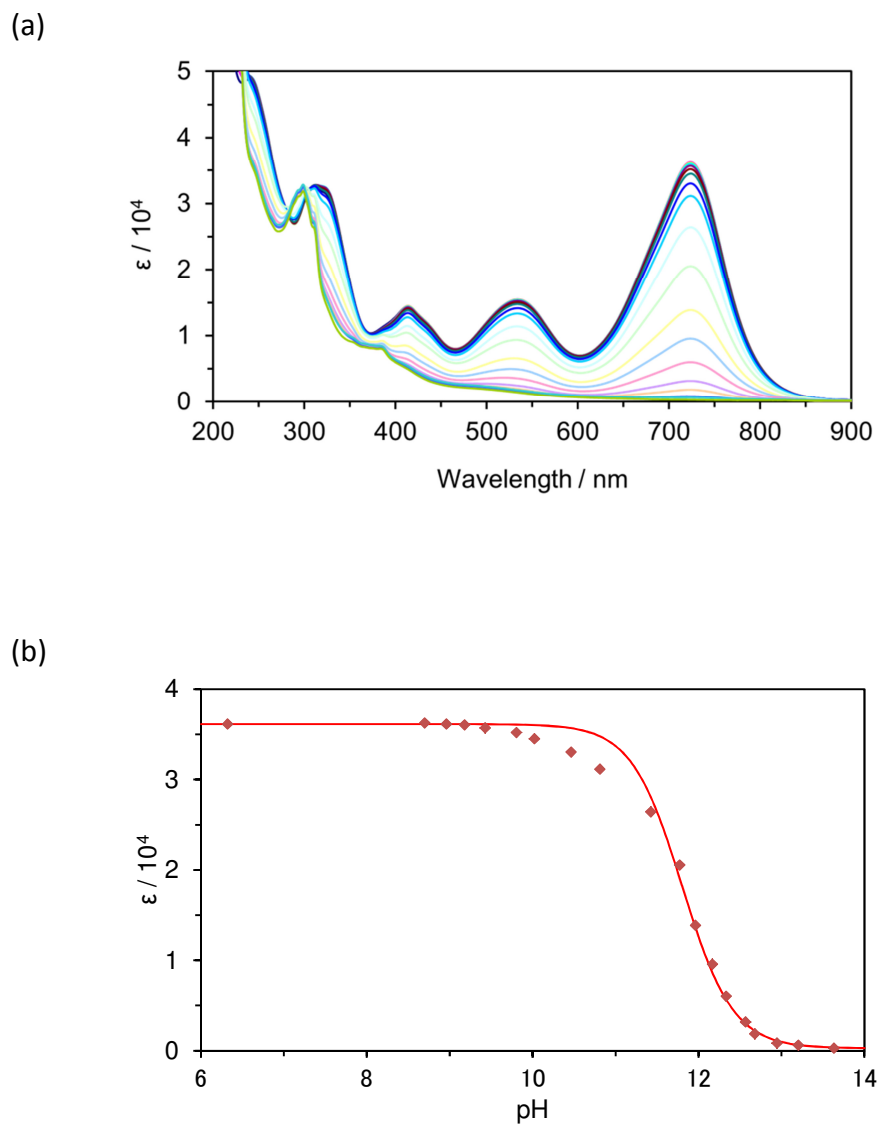


Figure S7. Continuous change in UV/Vis spectra of **11c⁺**: (a) change in UV/Vis spectra and (b) a plot of pH vs. absorbance at the longest wavelength absorption maximum in base titration in 50% water/acetonitrile solution.

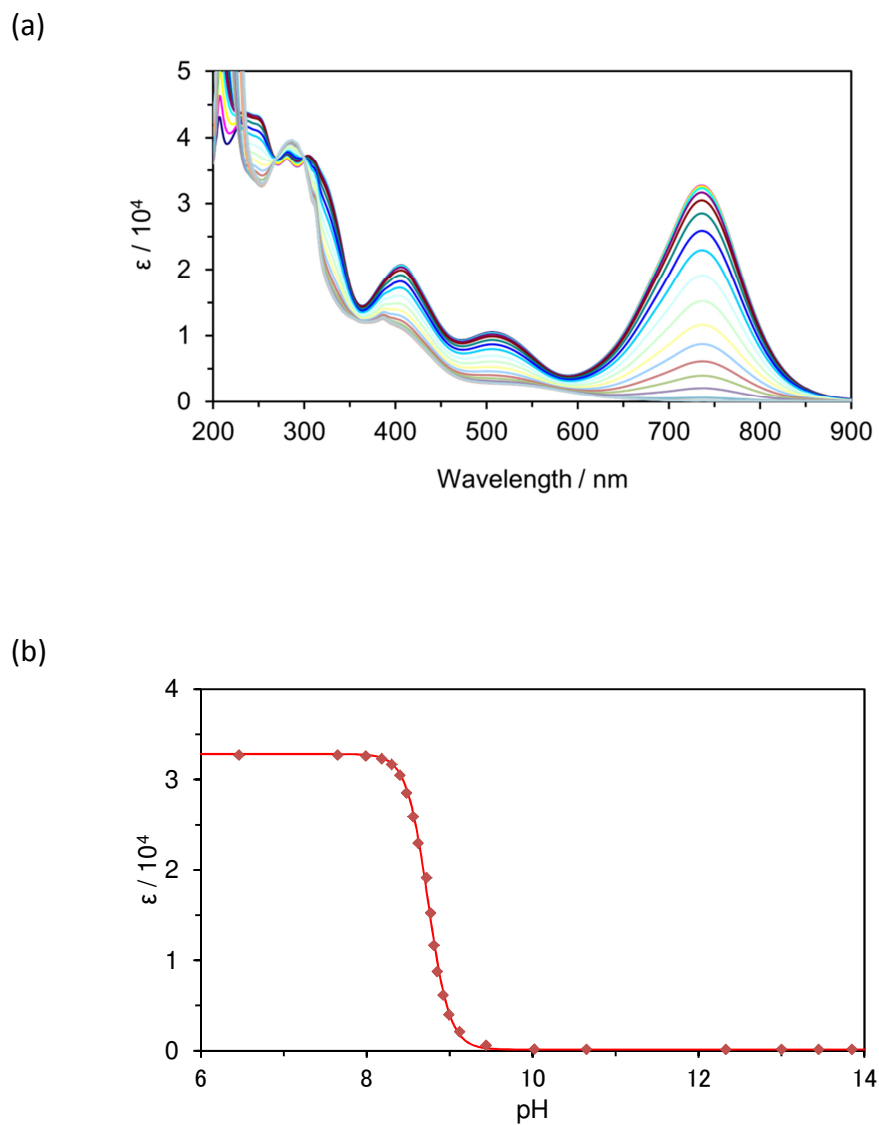


Figure S8. Continuous change in UV/Vis spectra of **11d**⁺: (a) change in UV/Vis spectra and (b) a plot of pH vs. absorbance at the longest wavelength absorption maximum in base titration in 50% water/acetonitrile solution.

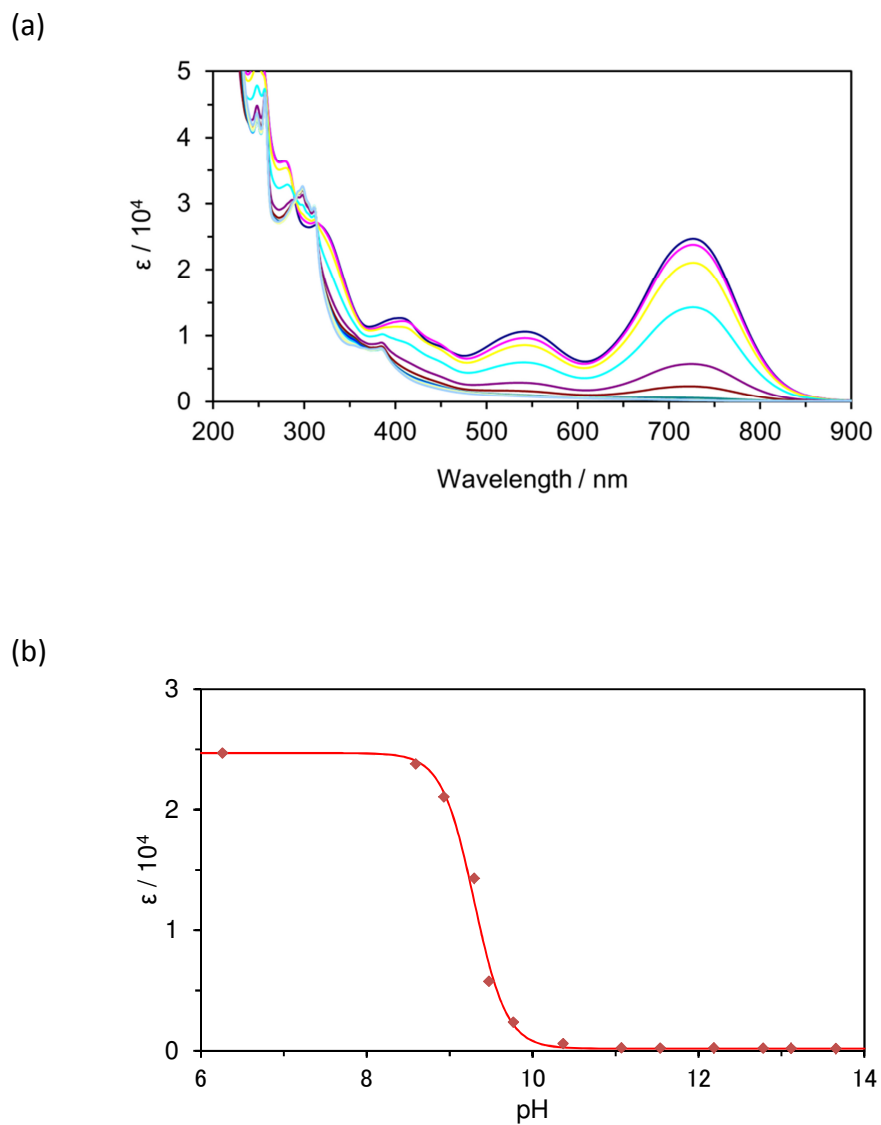


Figure S9. Continuous change in UV/Vis spectra of 14^+ : (a) change in UV/Vis spectra and (b) a plot of pH vs. absorbance at the longest wavelength absorption maximum in base titration in 50% water/acetonitrile solution.

3. CV and DPV waves of **5a⁺**, **5b⁺**, **8a⁺**, **8b⁺**, **11a-d⁺**, and **14⁺**Table S2. Reduction potentials^a of **5a⁺**, **5b⁺**, **8a⁺**, **8b⁺**, **11a-d⁺**, and **14⁺**

Sample	E_1^{red}	E_2^{red}	E_3^{red}	E_4^{red}	E_5^{red}	E_6^{red}
5a⁺	-0.59	-0.94	(-2.14)			
	(-0.55)	(-0.92)	(-2.09)			
5b⁺	-0.31	-0.79	(-1.47)	(-1.74)	(-1.77)	
	(-0.28)	(-0.76)	(-1.44)	(-1.68)	(-1.76)	
8a⁺	-0.63	-1.08	(-1.97)	(-2.08)		
	(-0.61)	(-1.06)	(-1.94)	(-2.03)	(-2.16)	
8b⁺	-0.36	-0.99	(-1.42)	(-1.67)	(-1.76)	
	(-0.34)	(-0.96)	(-1.38)	(-1.63)	(-1.74)	(-2.02)
11a⁺	-0.67	(-1.48)				
	(-0.64)	(-1.45)	(-2.03)	(-2.16)		
11b⁺	-0.37	(-1.19)	(-1.54)	(-1.64)	(-1.77)	
	(-0.34)	(-1.15)	(-1.51)	(-1.60)	(-1.74)	
11c⁺	-0.65	(-1.54)				
	(-0.62)	(-1.42)	(-1.87)	(-2.02)	(-2.16)	
11d⁺	-0.50	-0.86	(-1.57)	(-1.87)		
	(-0.48)	(-0.84)	(-1.54)	(-1.84)	(-2.04)	(-2.15)
14⁺	-0.49	(-1.12)				
	(-0.47)	(-1.08)	(-1.92)	(-2.00)	(-2.11)	(-2.22)

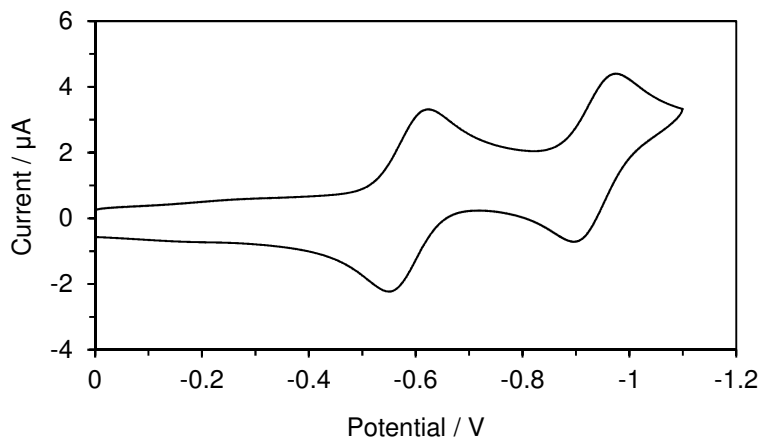
^a Redox potentials were measured by CV and DPV [V vs. Ag/AgNO₃, 1 mM in benzonitrile containing Et₄NClO₄ (0.1 M), Pt electrode (ID: 1.6 mm), scan rate 100 mV s⁻¹, and Fc/Fc⁺ = +0.15 V]. The peak potentials measured by DPV are shown in the second line with parentheses.

Table S3. Oxidation potentials^a of **5a⁺**, **5b⁺**, **8a⁺**, **8b⁺**, **11a–d⁺**, and **14⁺**

Sample	E_1^{ox}	E_2^{ox}	E_3^{ox}	E_4^{ox}
5a⁺	+0.94	(+1.44)		
	(+0.92)	(+1.41)		
5b⁺	(+1.38)			
	(+1.35)			
8a⁺	+0.95	(+1.33)	(+1.54)	(+1.71)
	(+0.93)	(+1.29)	(+1.48)	(+1.64)
8b⁺	(+1.43)	(+1.76)		
	(+1.36)	(+1.68)		
11a⁺	+0.84	(+1.40)		
	(+0.82)	(+1.30)		
11b⁺	(+1.27)	(+1.62)		
	(+1.24)	(+1.59)	(+1.77)	
11c⁺	+0.85			
	(+0.82)	(+1.41)	(+1.50)	
11d⁺	+0.88			
	(+0.86)	(+1.38)	(+1.64)	
14⁺	+0.93	(+1.48)		
	(+0.90)	(+1.41)		

^a Redox potentials were measured by CV and DPV [V vs. Ag/AgNO₃, 1 mM in benzonitrile containing Et₄NClO₄ (0.1 M), Pt electrode (ID: 1.6 mm), scan rate 100 mV s⁻¹, and Fc/Fc⁺ = +0.15 V]. The peak potentials measured by DPV are shown in the second line with parentheses.

(a)



(b)

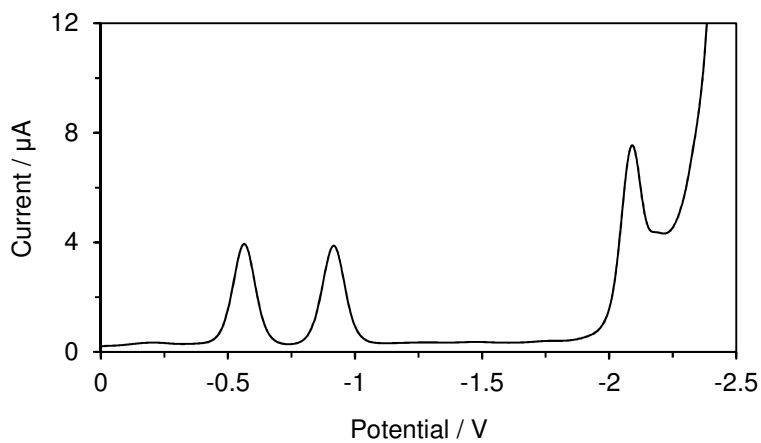


Figure S10. Voltammograms of $5a^+$: (a) reduction wave on CV and (b) reduction wave of on DPV in benzonitrile (1 mM) containing Et_4NClO_4 (0.1 M) as a supporting electrolyte; scan rate, 100 mV s^{-1} .

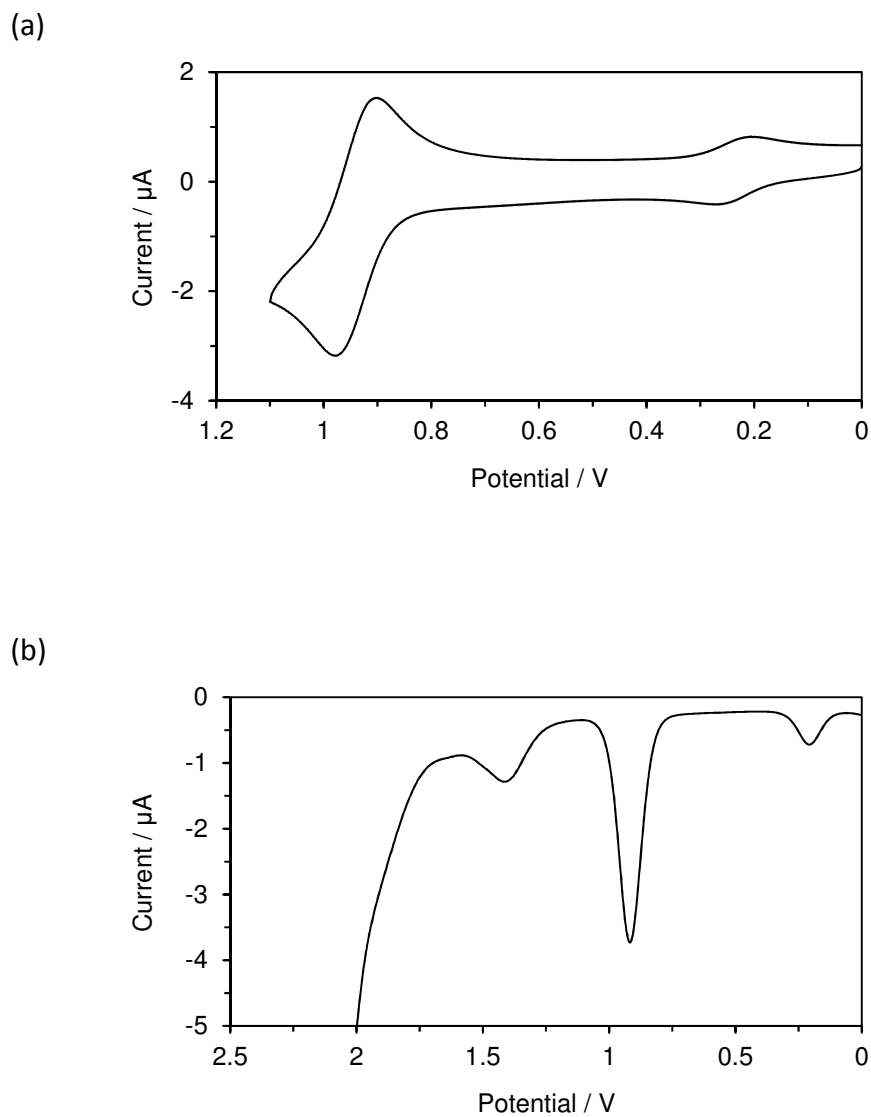
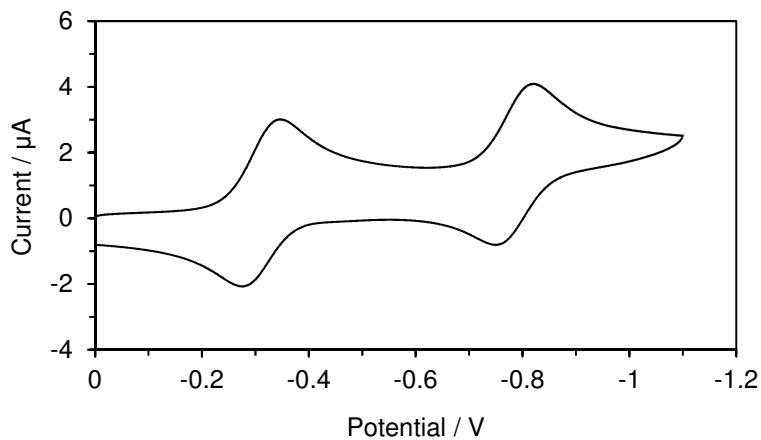


Figure S11. Voltammograms of $5a^+$: (a) oxidation wave on CV and (b) oxidation wave on DPV in benzonitrile (1 mM) containing Et_4NClO_4 (0.1 M) as a supporting electrolyte; scan rate, 100 mV s^{-1} .

(a)



(b)

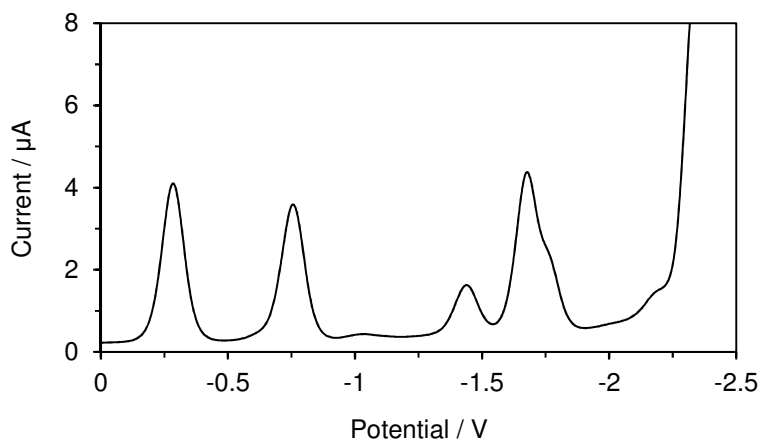


Figure S12. Voltammograms of $5b^+$: (a) reduction wave on CV and (b) reduction wave on DPV in benzonitrile (1 mM) containing Et_4NClO_4 (0.1 M) as a supporting electrolyte; scan rate, 100 mV s^{-1} .

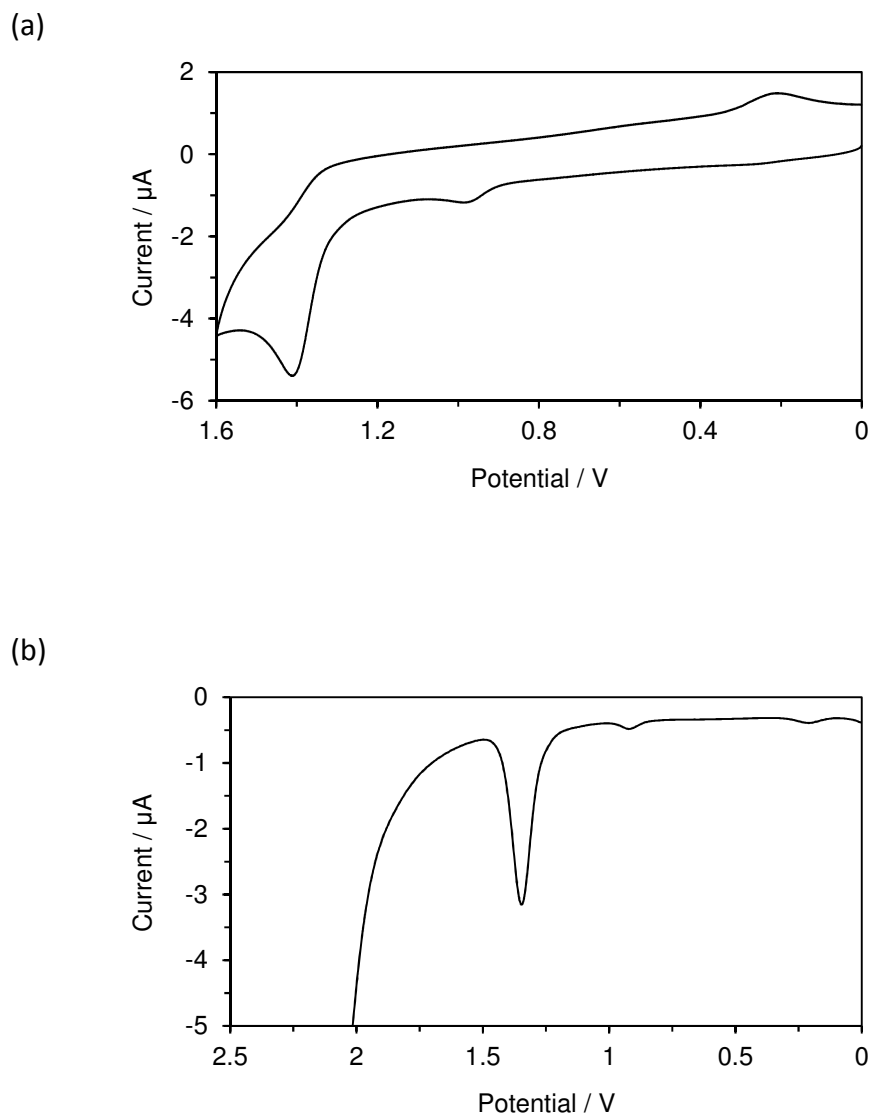


Figure S13. Voltammograms of $5b^+$: (a) reduction wave on CV and (b) oxidation wave on DPV in benzonitrile (1 mM) containing Et_4NClO_4 (0.1 M) as a supporting electrolyte; scan rate, 100 mV s^{-1} .

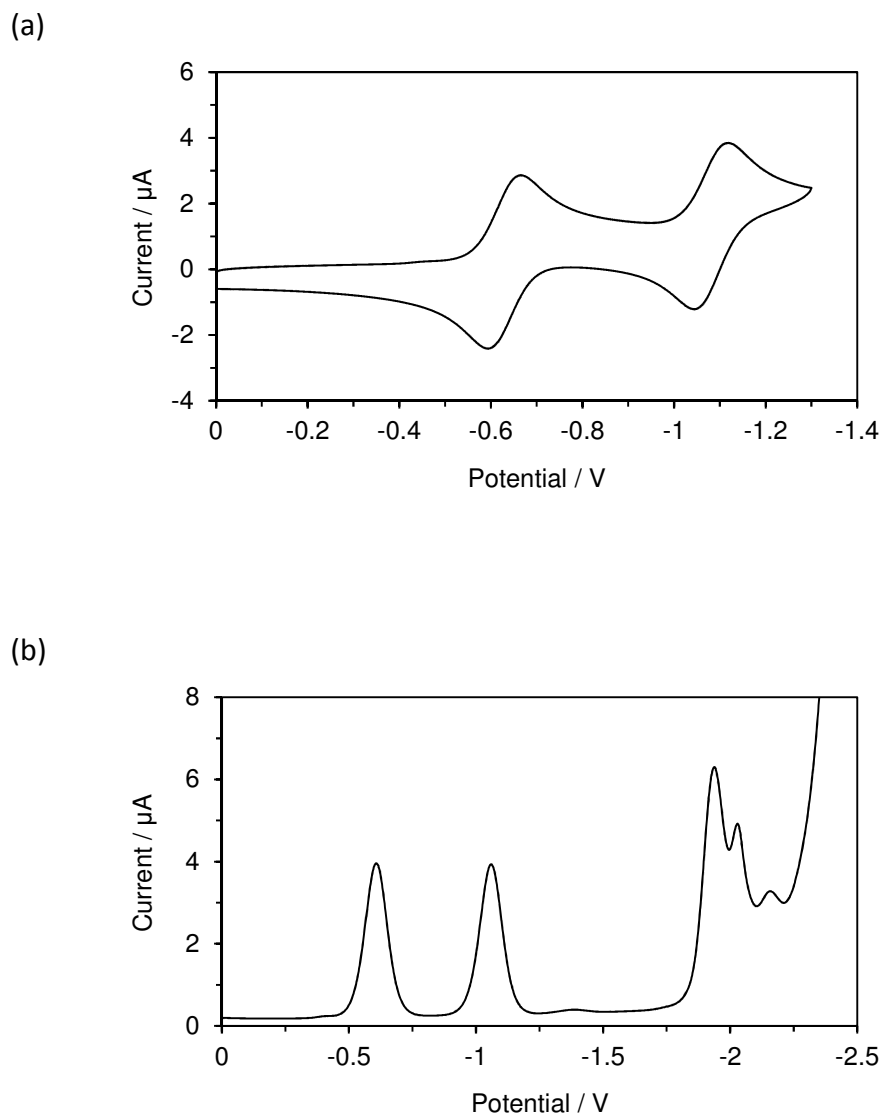


Figure S14. Voltammograms of $8a^+$: (a) reduction wave on CV and (b) oxidation wave on DPV in benzonitrile (1 mM) containing Et_4NClO_4 (0.1 M) as a supporting electrolyte; scan rate, 100 mV s^{-1} .

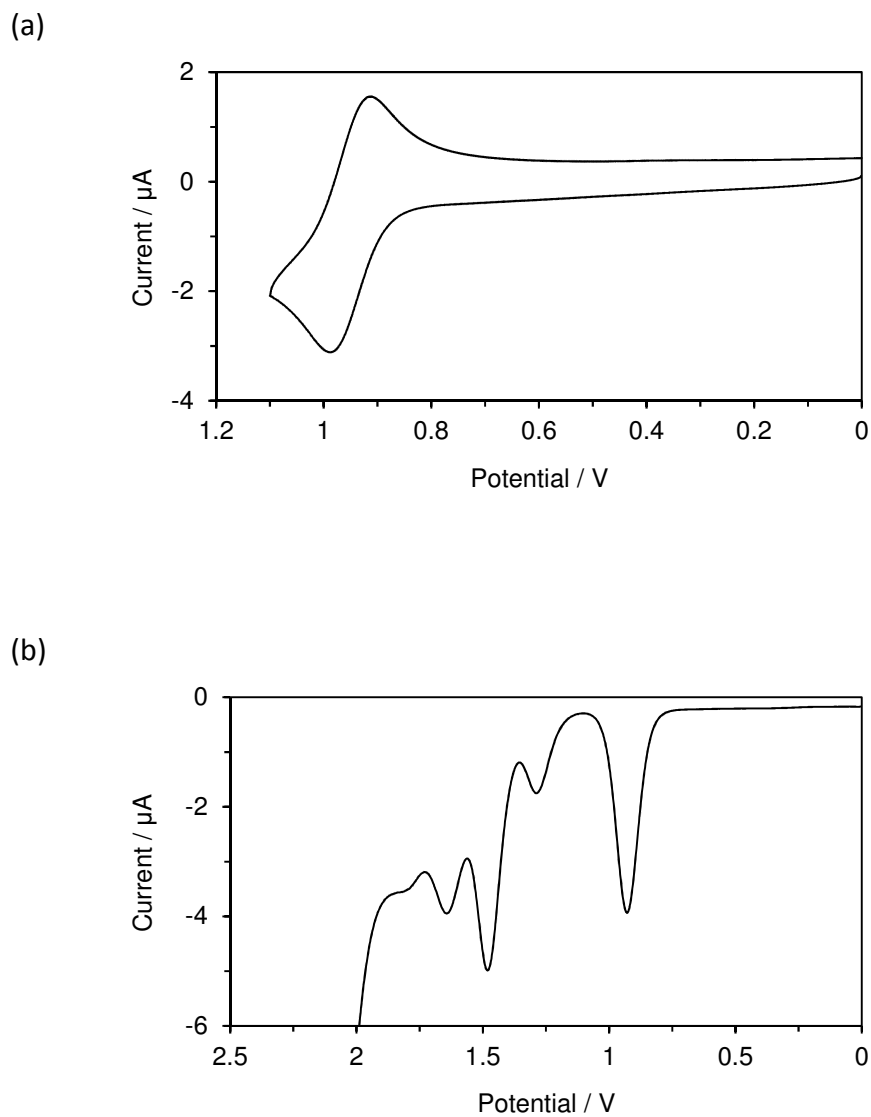
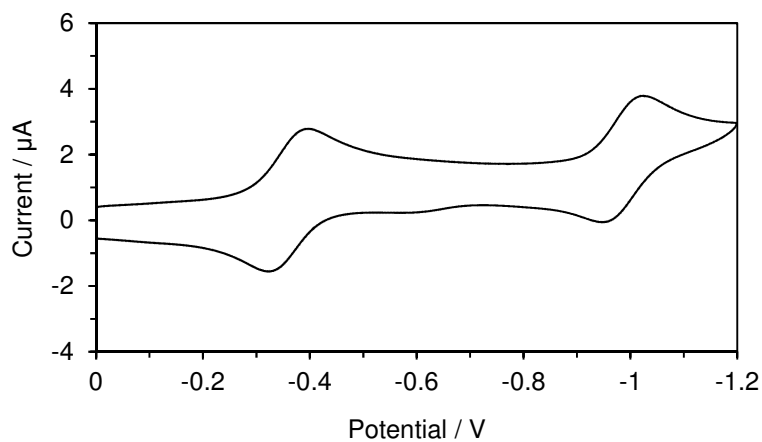


Figure S15. Voltammograms of $8a^+$: (a) reduction wave on CV and (b) oxidation wave on DPV in benzonitrile (1 mM) containing Et_4NClO_4 (0.1 M) as a supporting electrolyte; scan rate, 100 mV s^{-1} .

(a)



(b)

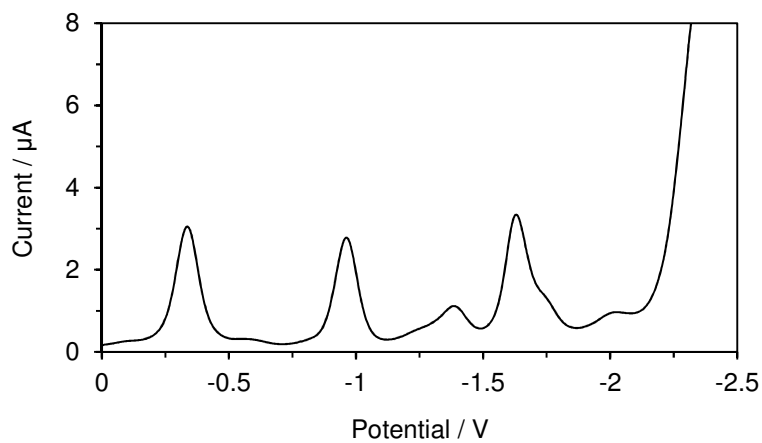


Figure S16. Voltammograms of $8b^+$: (a) reduction wave on CV and (b) oxidation wave on DPV in benzonitrile (1 mM) containing Et_4NClO_4 (0.1 M) as a supporting electrolyte; scan rate, 100 mV s^{-1} .

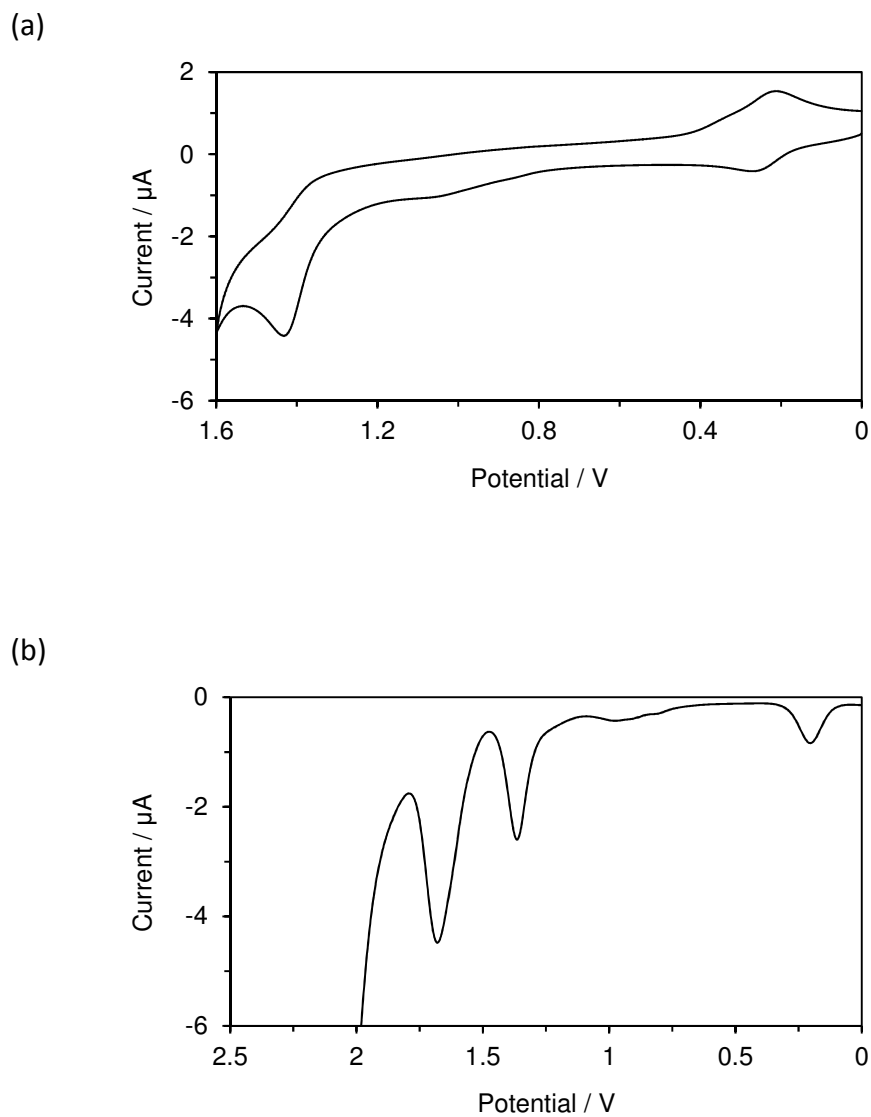


Figure S17. Voltammograms of $8b^+$: (a) reduction wave on CV and (b) oxidation wave on DPV in benzonitrile (1 mM) containing Et_4NClO_4 (0.1 M) as a supporting electrolyte; scan rate, 100 mV s^{-1} .

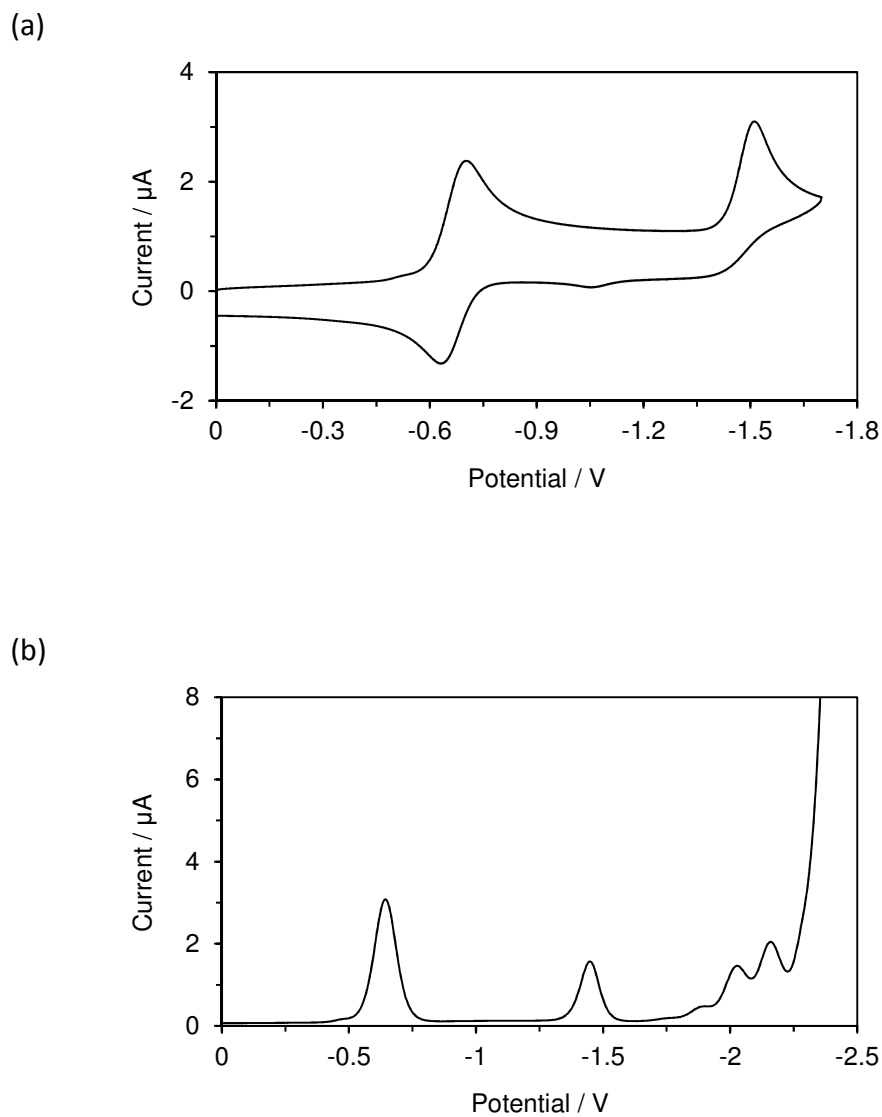


Figure S18. Voltammograms of **11a**⁺: (a) reduction wave on CV and (b) oxidation wave on DPV in benzonitrile (1 mM) containing Et₄NClO₄ (0.1 M) as a supporting electrolyte; scan rate, 100 mV s⁻¹.

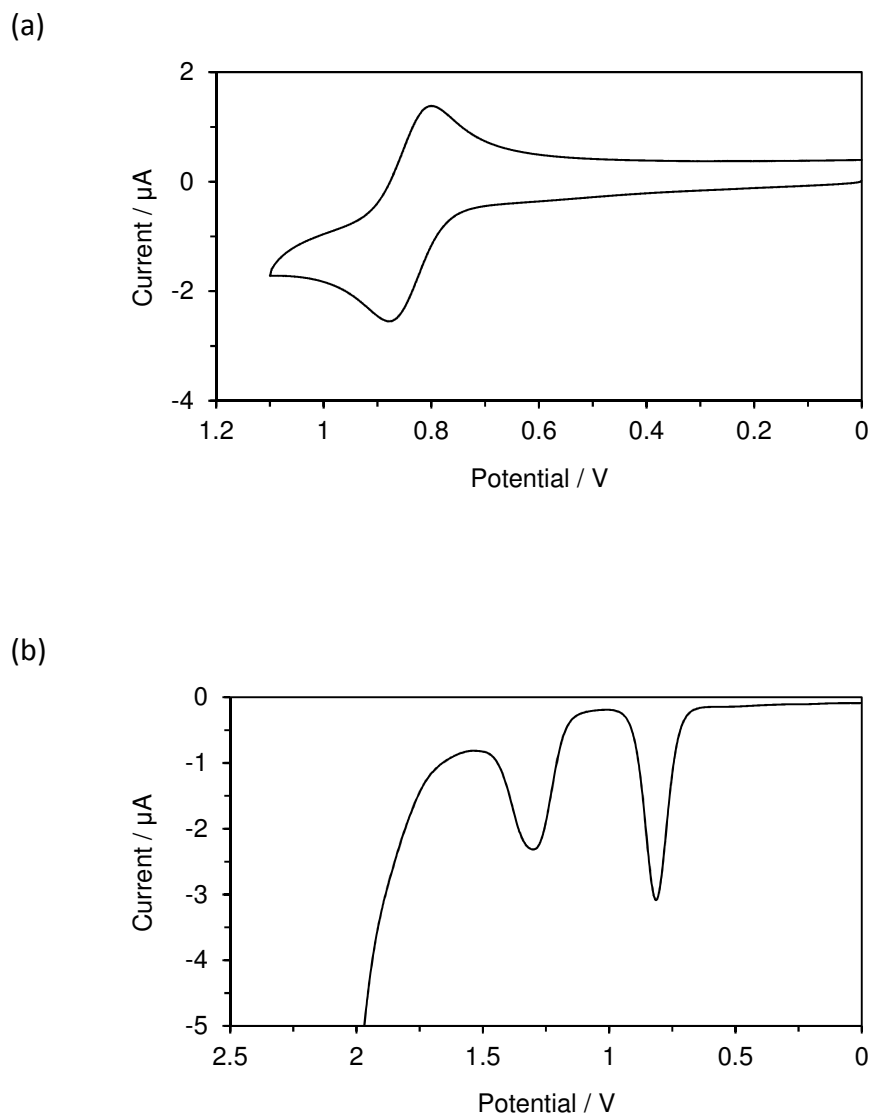


Figure S19. Voltammograms of $11a^+$: (a) reduction wave on CV and (b) oxidation wave on DPV in benzonitrile (1 mM) containing Et_4NClO_4 (0.1 M) as a supporting electrolyte; scan rate, 100 mV s^{-1} .

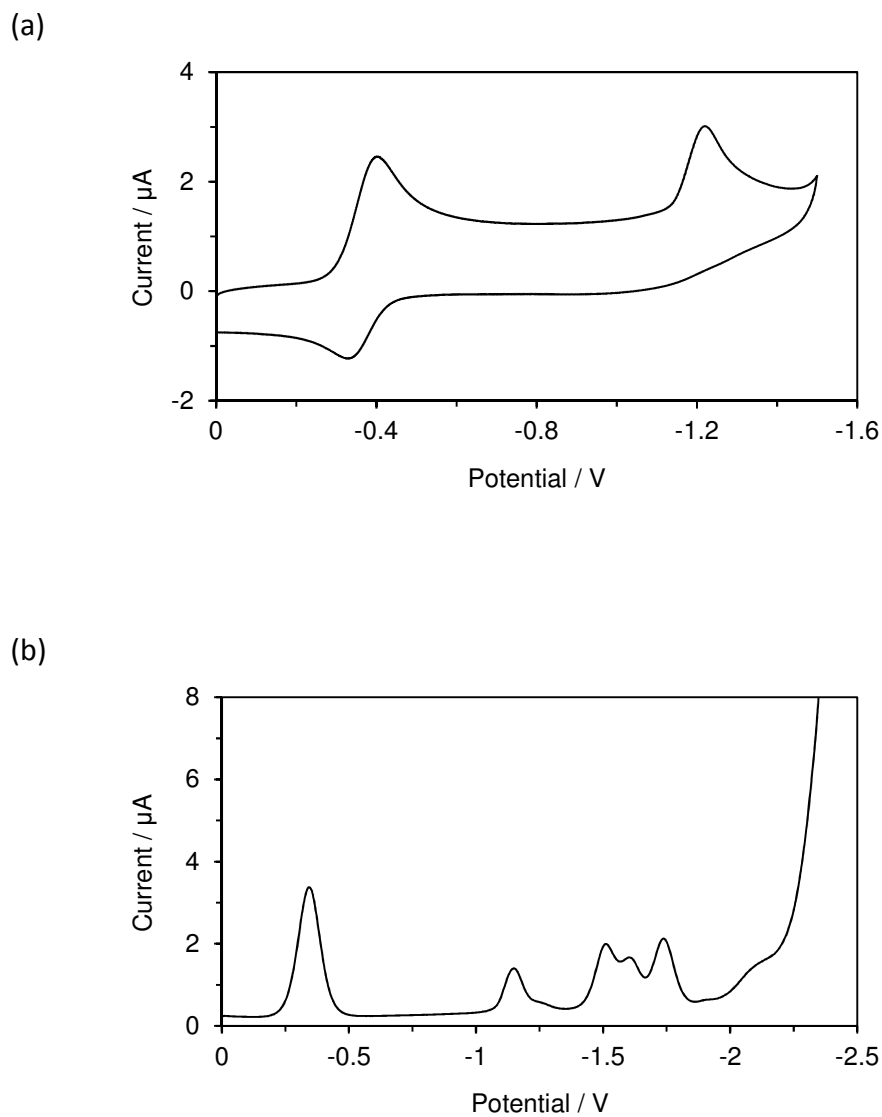
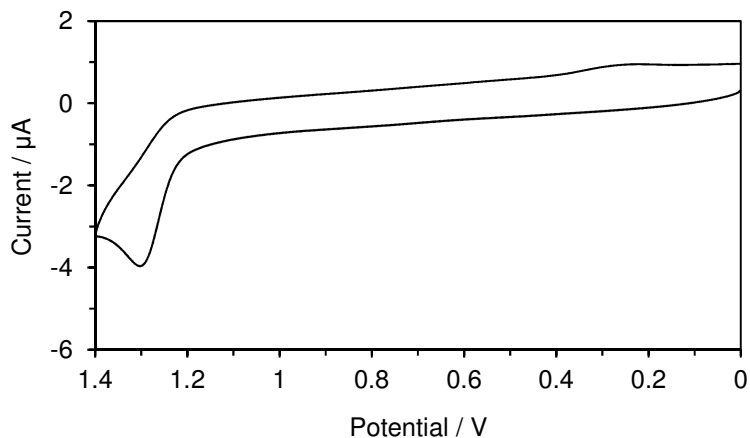


Figure S20. Voltammograms of **11b**⁺: (a) reduction wave on CV and (b) oxidation wave on DPV in benzonitrile (1 mM) containing Et₄NClO₄ (0.1 M) as a supporting electrolyte; scan rate, 100 mV s⁻¹.

(a)



(b)

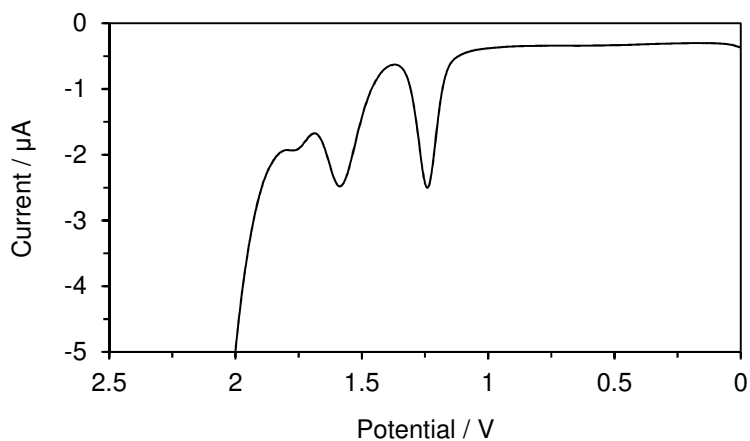


Figure S21. Voltammograms of $11b^+$: (a) reduction wave on CV and (b) oxidation wave on DPV in benzonitrile (1 mM) containing Et_4NClO_4 (0.1 M) as a supporting electrolyte; scan rate, 100 mV s^{-1} .

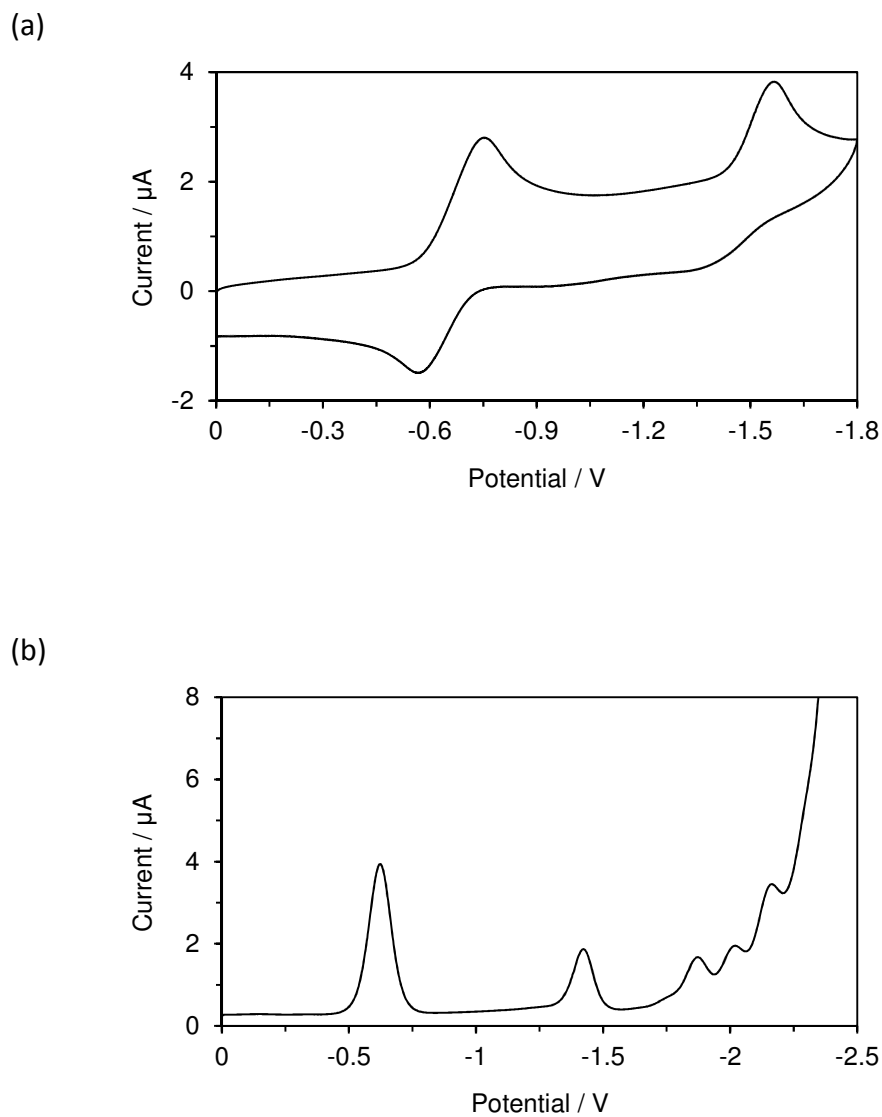


Figure S22. Voltammograms of $11c^+$: (a) reduction wave on CV and (b) oxidation wave on DPV in benzonitrile (1 mM) containing Et_4NClO_4 (0.1 M) as a supporting electrolyte; scan rate, 100 mV s^{-1} .

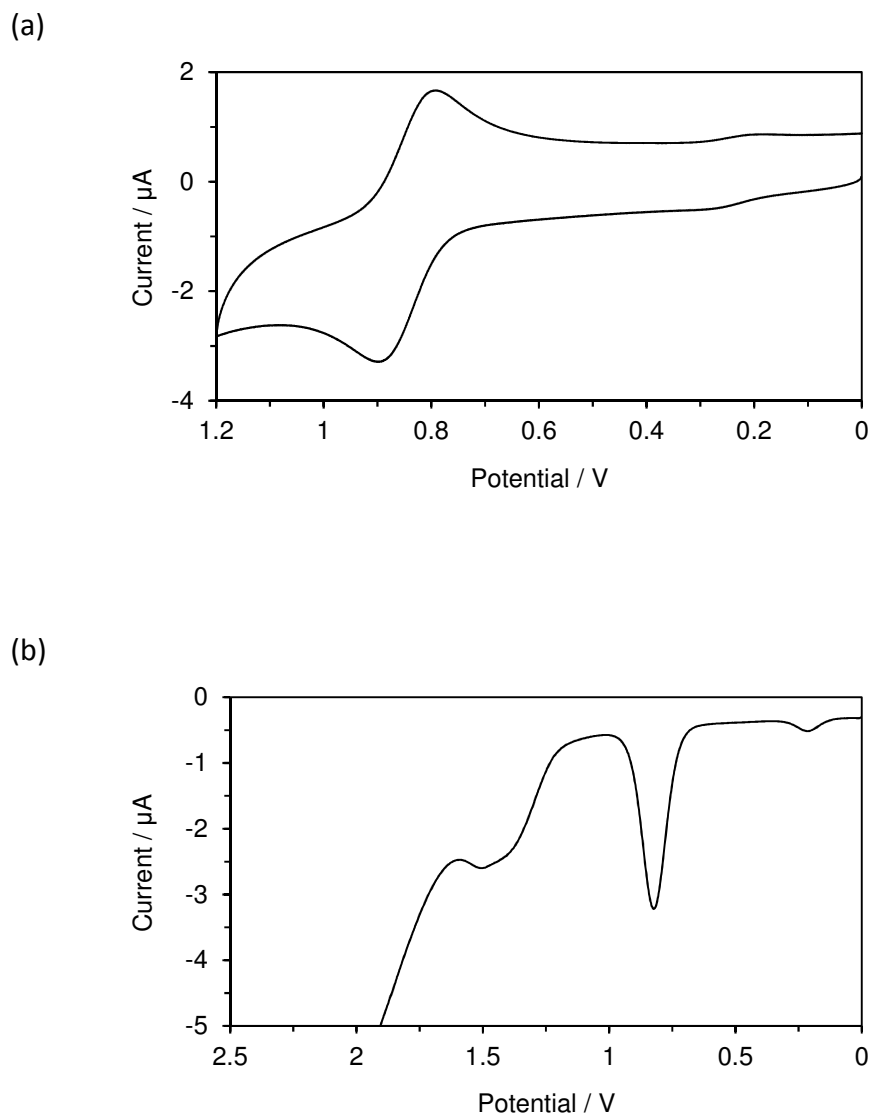


Figure S23. Voltammograms of $11c^+$: (a) reduction wave on CV and (b) oxidation wave on DPV in benzonitrile (1 mM) containing Et_4NClO_4 (0.1 M) as a supporting electrolyte; scan rate, 100 mV s^{-1} .

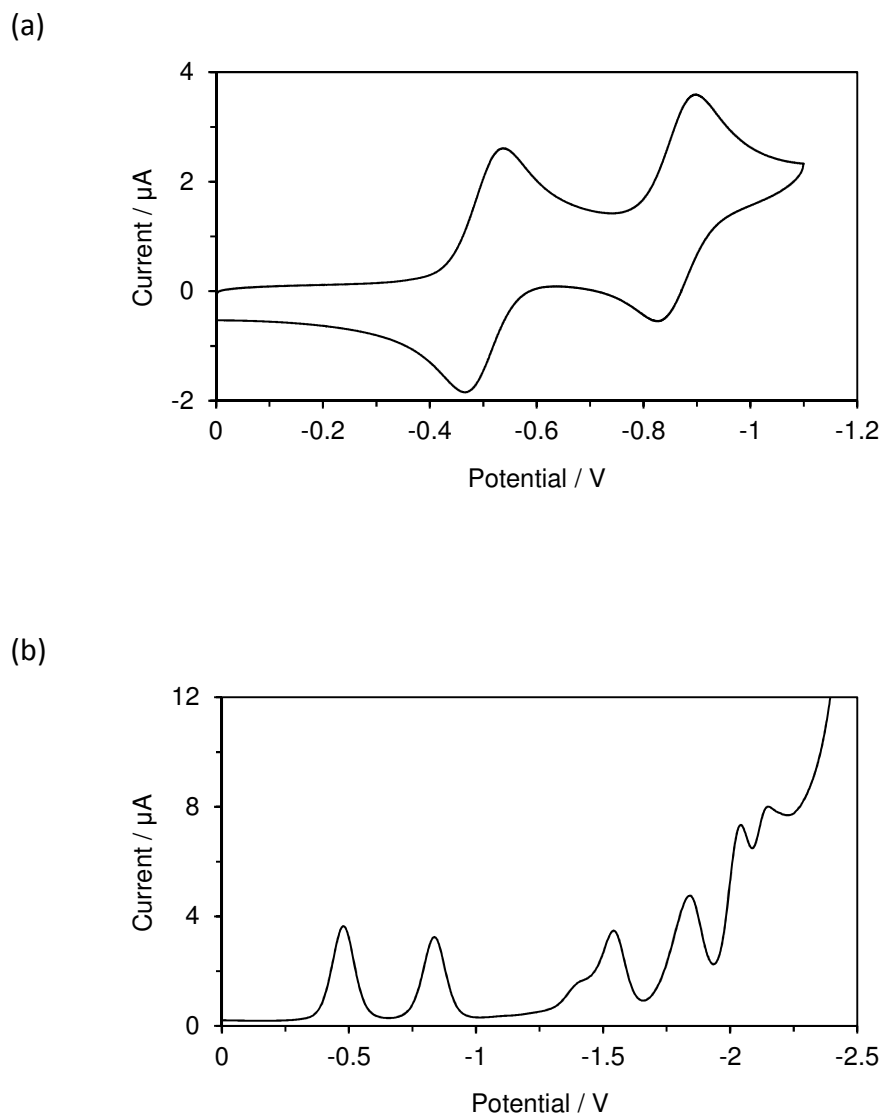


Figure S24. Voltammograms of **11d**⁺: (a) reduction wave on CV and (b) oxidation wave on DPV in benzonitrile (1 mM) containing Et₄NClO₄ (0.1 M) as a supporting electrolyte; scan rate, 100 mV s⁻¹.

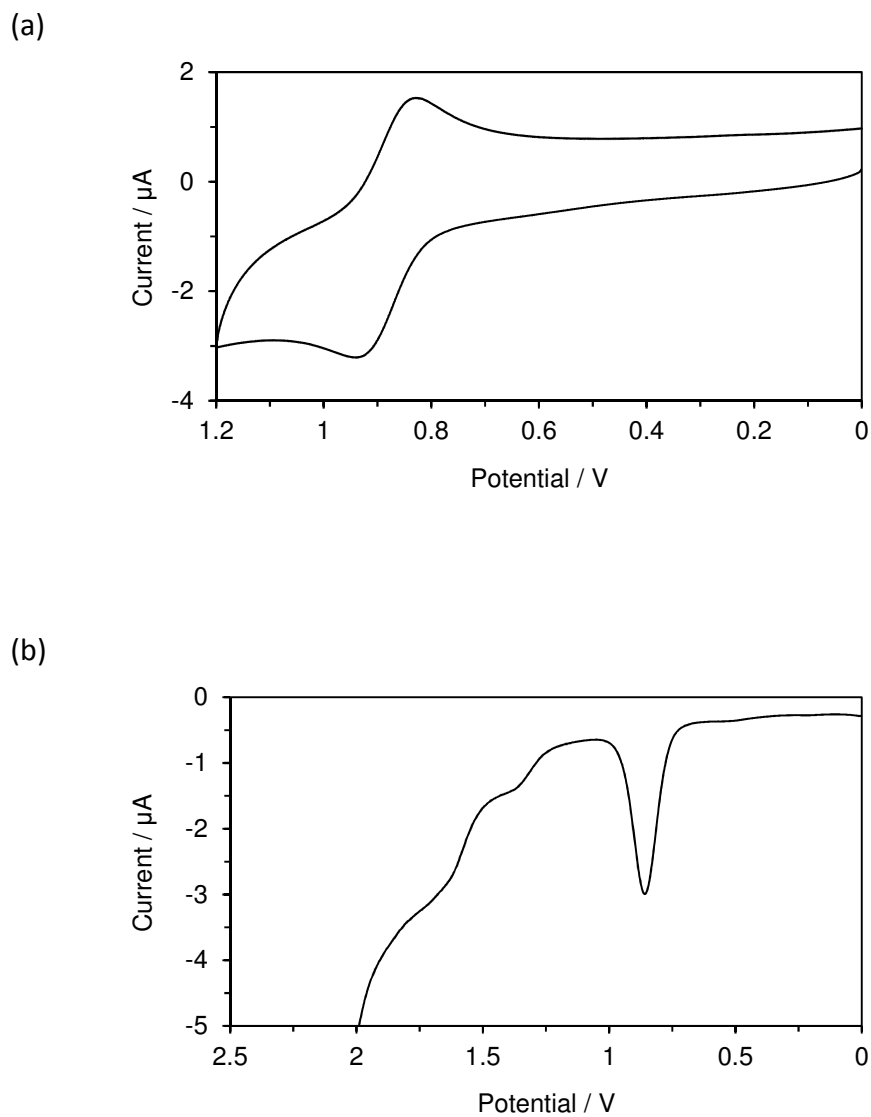


Figure S25. Voltammograms of **11d**⁺: (a) reduction wave on CV and (b) oxidation wave on DPV in benzonitrile (1 mM) containing Et₄NClO₄ (0.1 M) as a supporting electrolyte; scan rate, 100 mV s⁻¹.

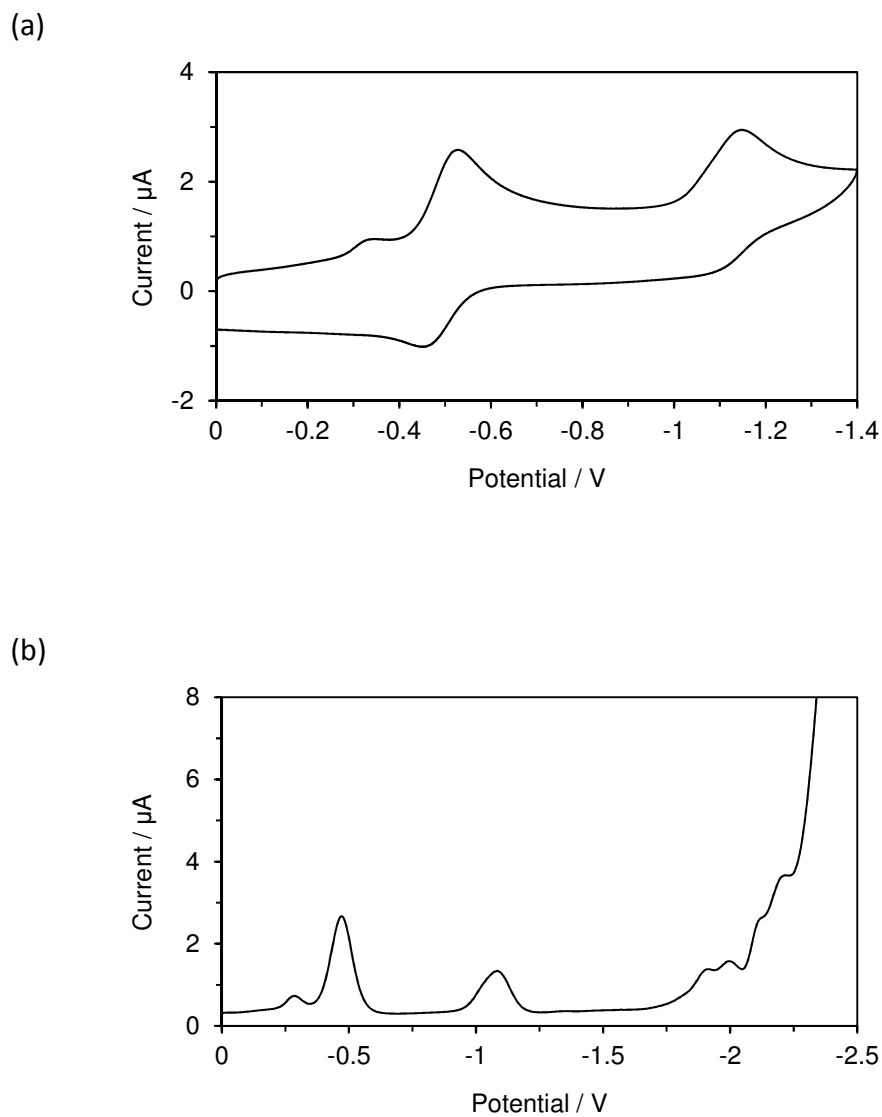


Figure S26. Voltammograms of 14^+ : (a) reduction wave on CV and (b) oxidation wave on DPV in benzonitrile (1 mM) containing Et_4NClO_4 (0.1 M) as a supporting electrolyte; scan rate, 100 mV s^{-1} .

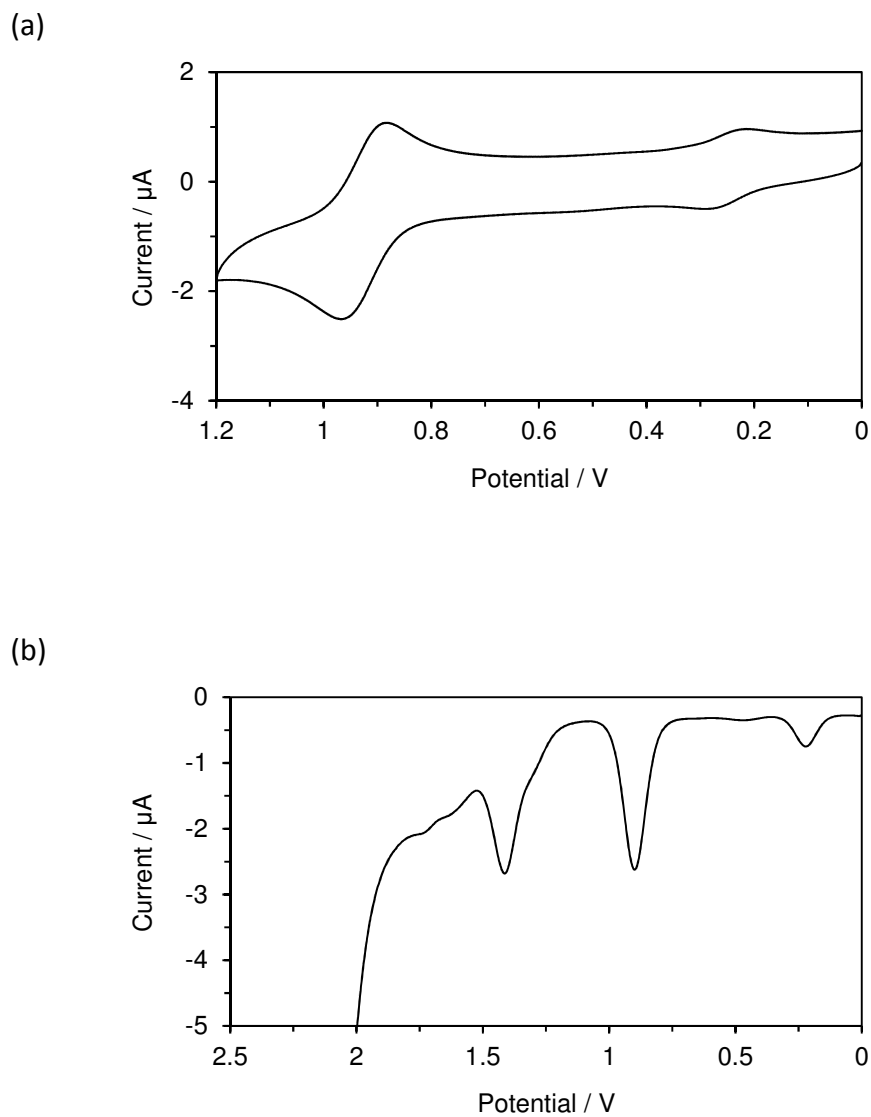


Figure S27. Voltammograms of 14^+ : (a) reduction wave on CV and (b) oxidation wave on DPV in benzonitrile (1 mM) containing Et_4NClO_4 (0.1 M) as a supporting electrolyte; scan rate, 100 mV s^{-1} .

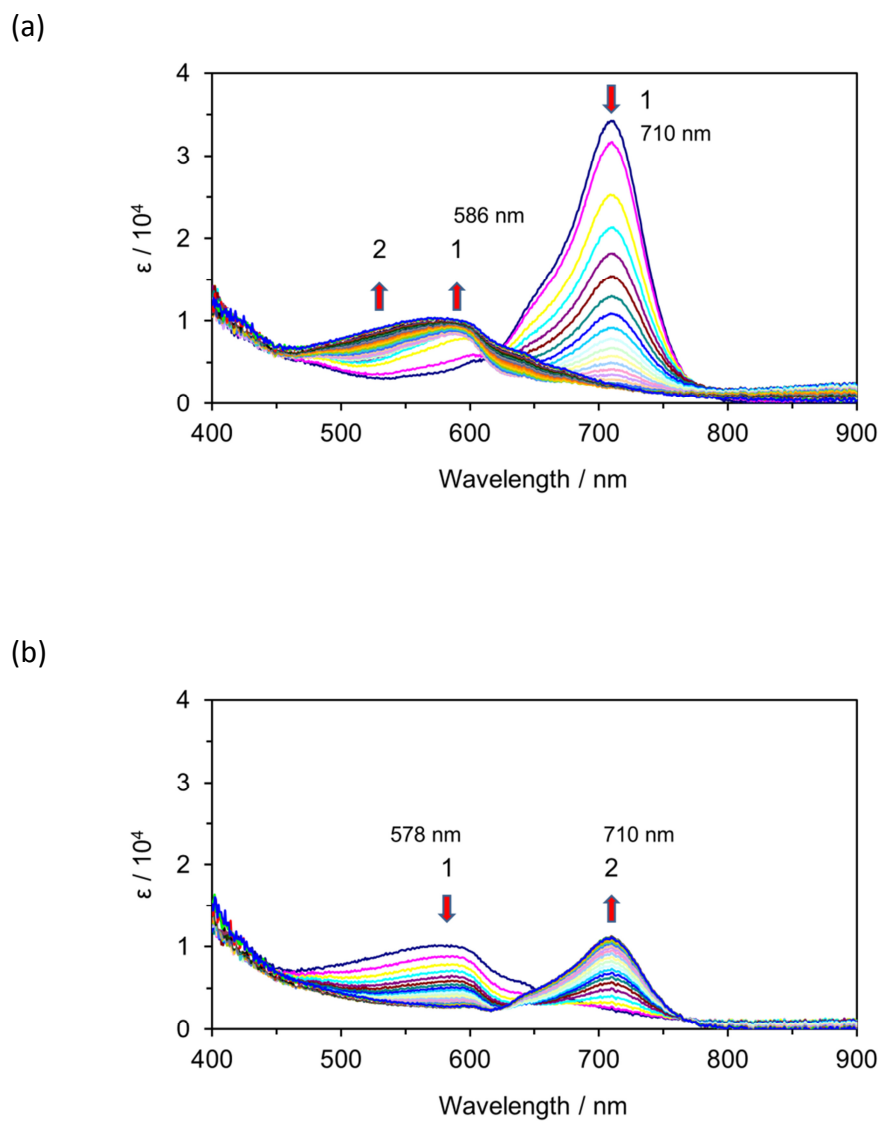
4. Spectroelectrograms of $5a^+$, $5b^+$, $8a^+$, $8b^+$, $11a-d^+$, and 14^+ 

Figure S28. Continuous change in the visible spectrum of $5a^+$: (a) constant-current electrochemical reduction ($70 \mu\text{A}$) and (b) reverse oxidation of the reduced species ($70 \mu\text{A}$) in benzonitrile ($2.5 \times 10^{-4} \text{ M}$, 2 mL) containing Et_4NClO_4 (0.1 M) at 1 min intervals.

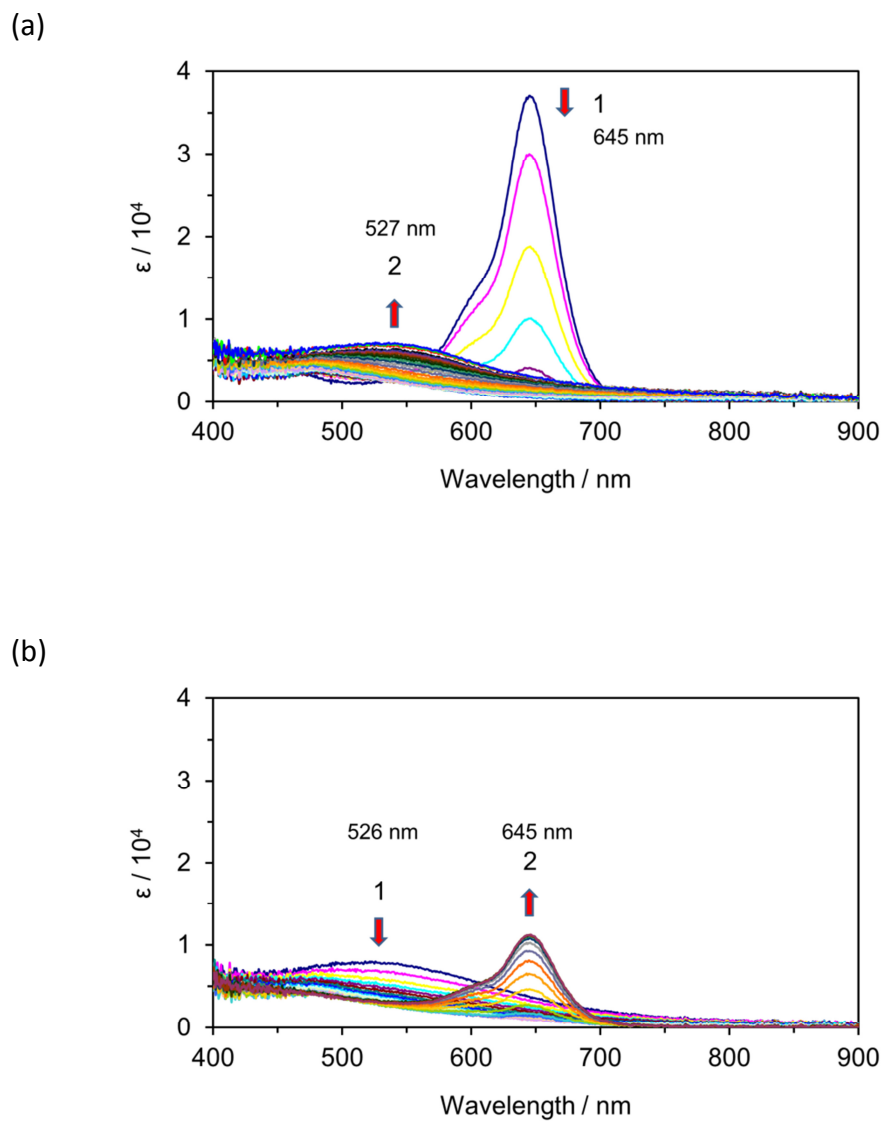


Figure S29. Continuous change in the visible spectrum of **5b**⁺: (a) constant-current electrochemical reduction (70 μ A) and (b) reverse oxidation of the reduced species (70 μ A) in benzonitrile (2.6×10^{-4} M, 2 mL) containing Et_4NClO_4 (0.1 M) at 1 min intervals.

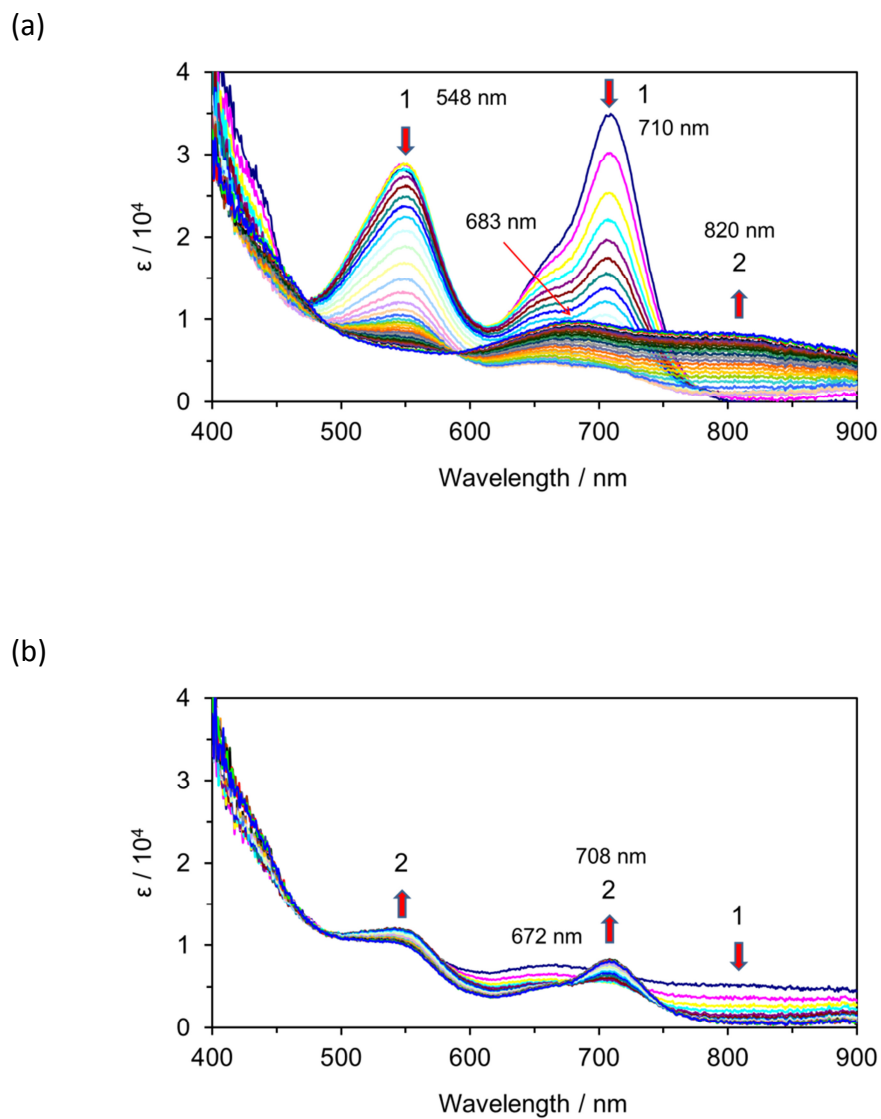


Figure S30. Continuous change in the visible spectrum of **8a⁺**: (a) constant-current electrochemical reduction (70 μ A) and (b) reverse oxidation of the reduced species (70 μ A) in benzonitrile (2.2×10^{-4} M, 2 mL) containing Et_4NClO_4 (0.1 M) at 1 min intervals.

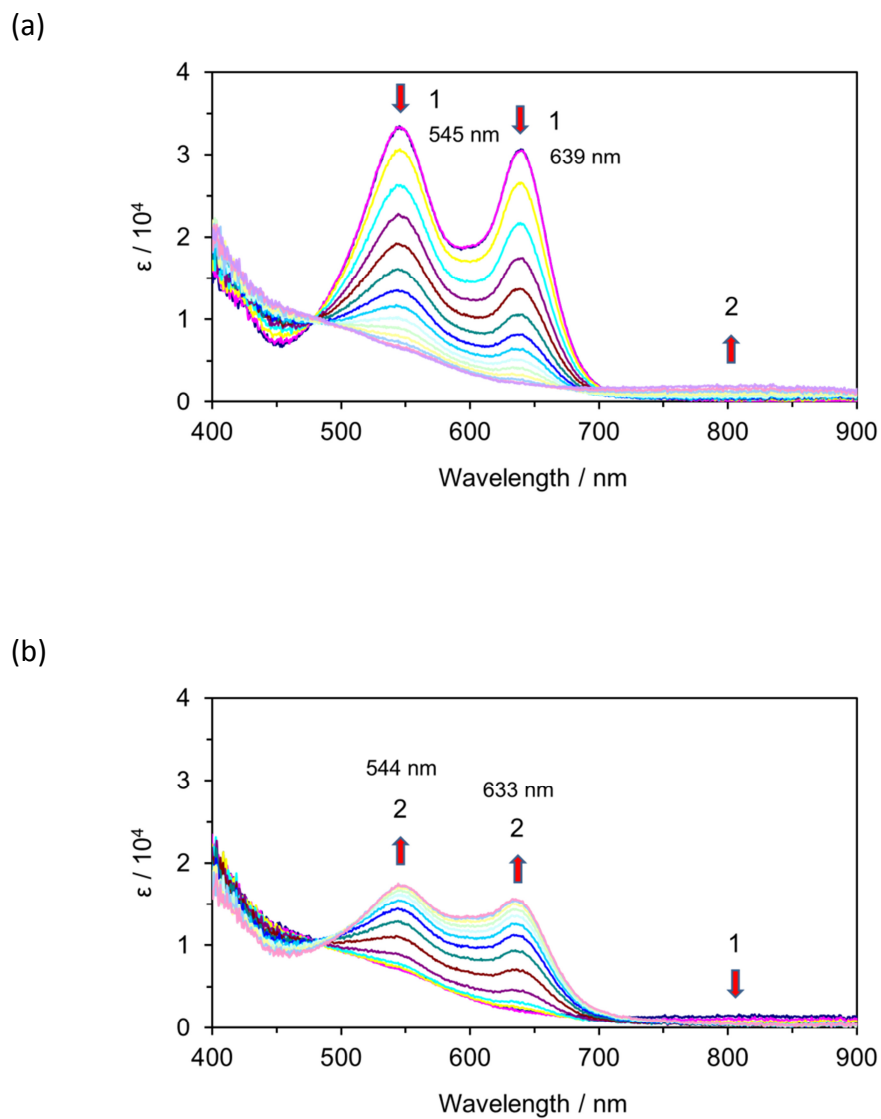


Figure S31. Continuous change in the visible spectrum of **8b**⁺: (a) constant-current electrochemical reduction (60 uA) and (b) reverse oxidation of the reduced species (60 uA) in benzonitrile (2.7×10^{-5} M, 2 mL) containing Et₄NClO₄ (0.1 M) at 1 min intervals.

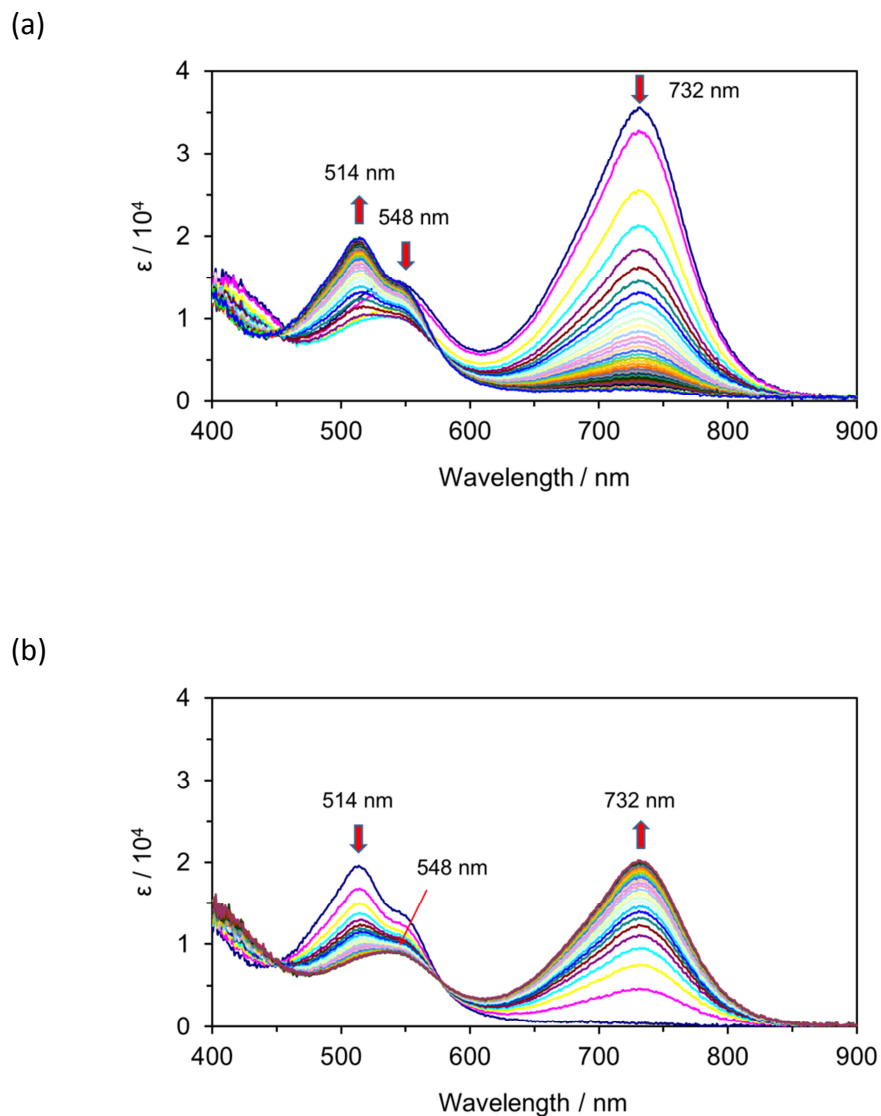


Figure S32. Continuous change in the visible spectrum of $11a^+$: (a) constant-current electrochemical reduction (70 μA) and (b) reverse oxidation of the reduced species (70 μA) in benzonitrile (2.9×10^{-4} M, 2 mL) containing Et_4NClO_4 (0.1 M) at 1 min intervals.

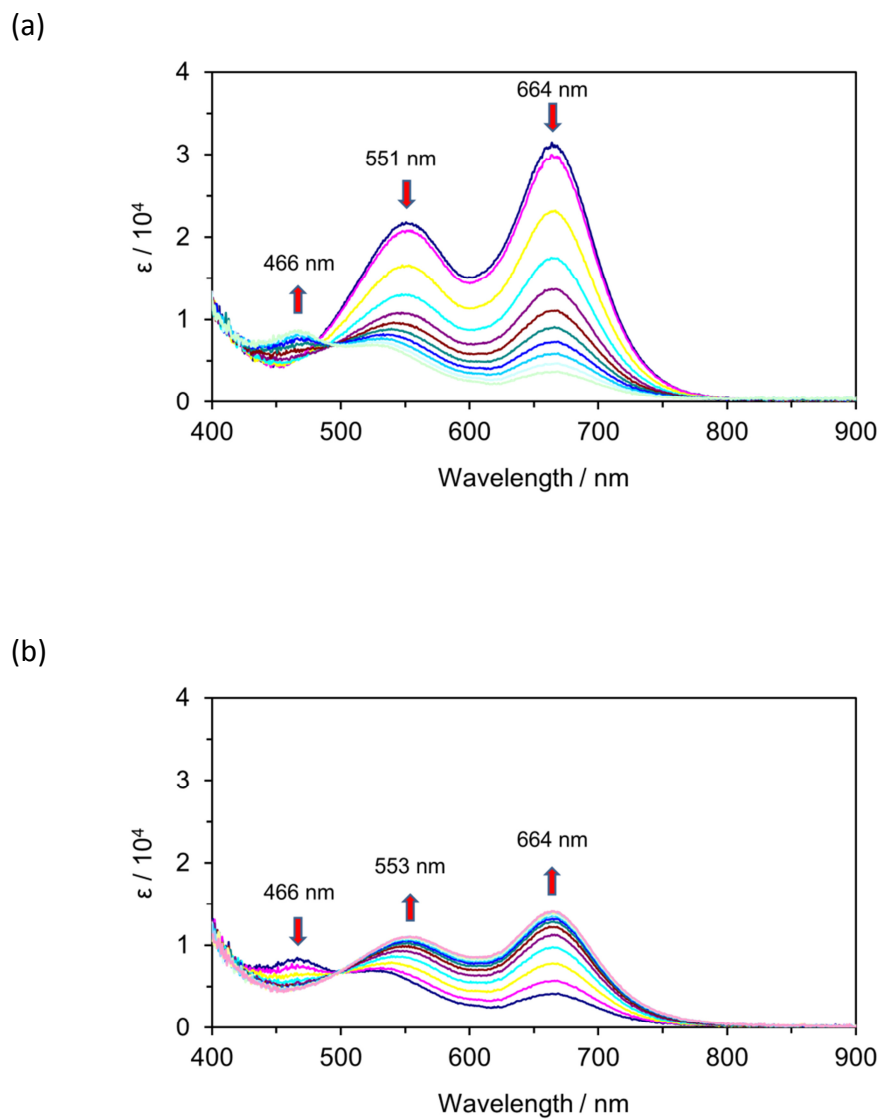


Figure S33. Continuous change in the visible spectrum of **11b**⁺: (a) constant-current electrochemical reduction (70 μ A) and (b) reverse oxidation of the reduced species (70 μ A) in benzonitrile (4.1×10^{-5} M, 2 mL) containing Et_4NClO_4 (0.1 M) at 1 min intervals.

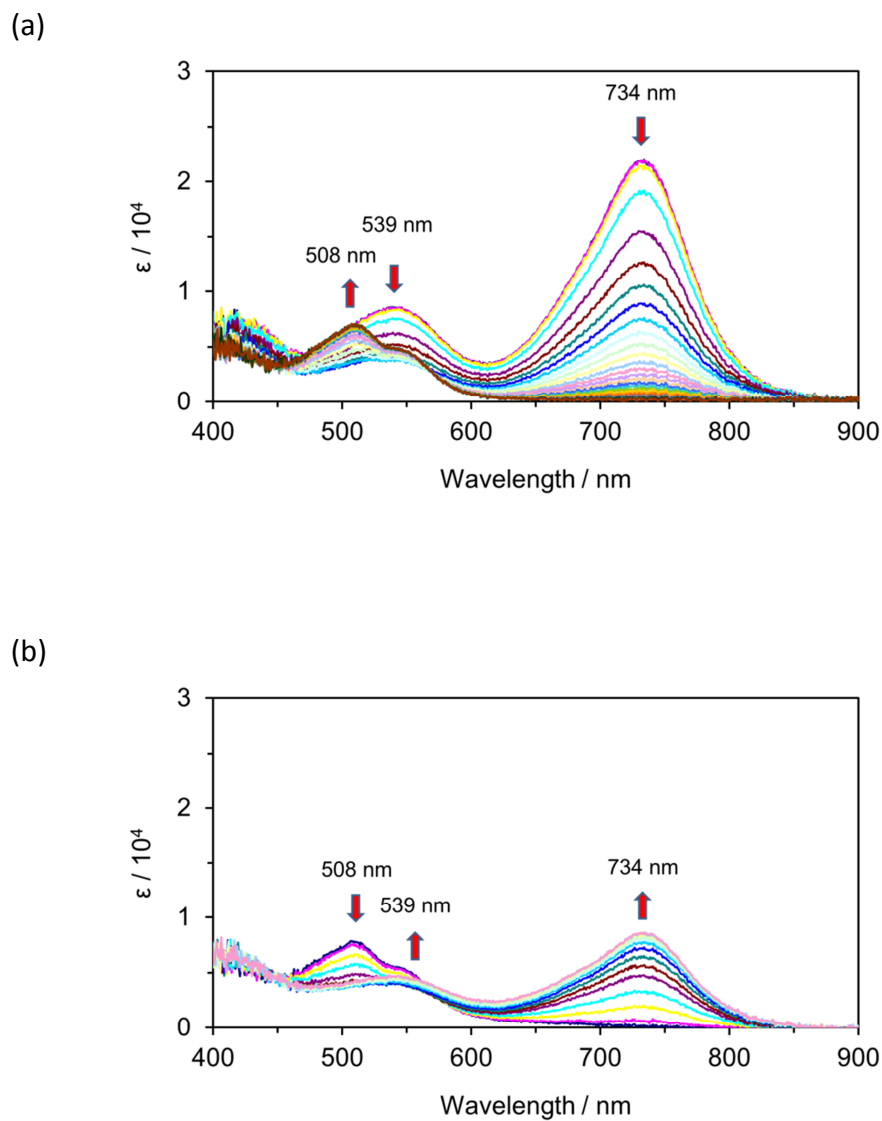


Figure S34. Continuous change in the visible spectrum of **11c⁺**: (a) constant-current electrochemical reduction (70 μA) and (b) reverse oxidation of the reduced species (70 μA) in benzonitrile (2.7×10^{-4} M, 2 mL) containing Et_4NClO_4 (0.1 M) at 1 min intervals.

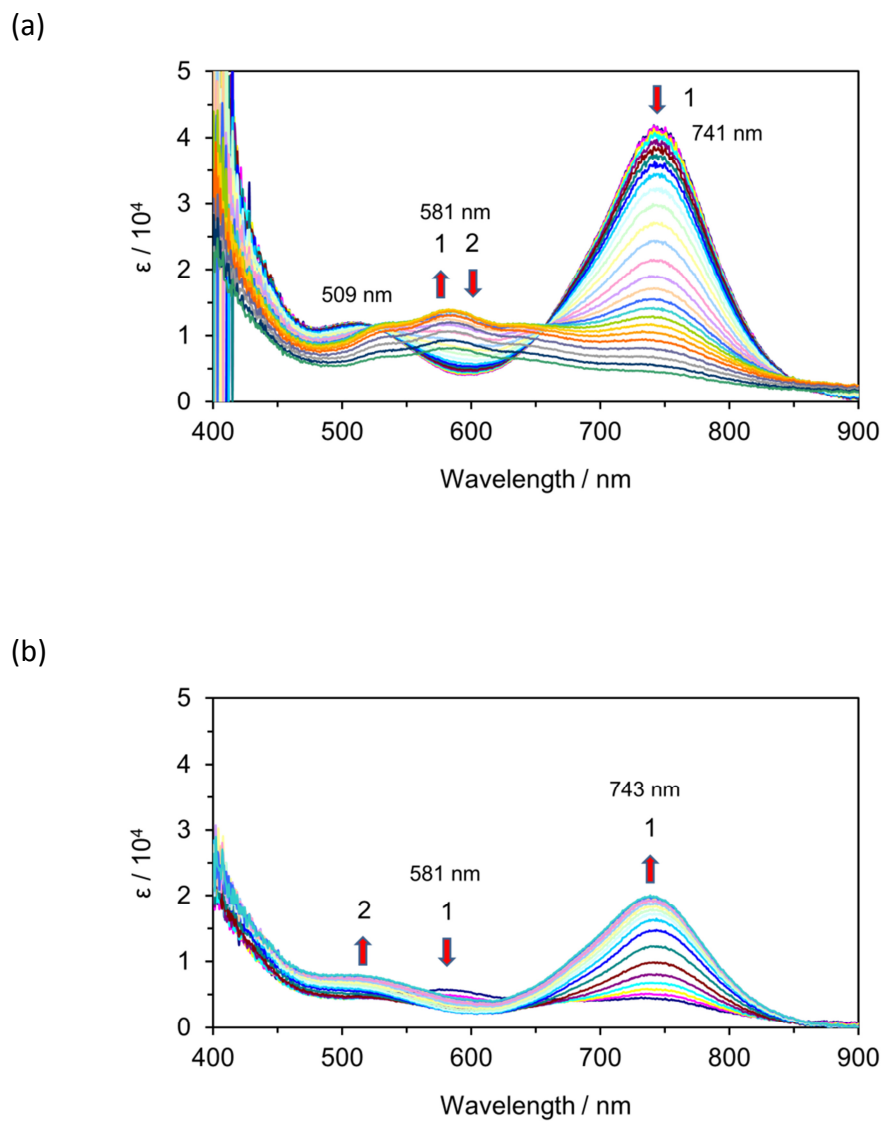


Figure S35. Continuous change in the visible spectrum of **11d**⁺: (a) constant-current electrochemical reduction (30 μA) and (b) reverse oxidation of the reduced species (30 μA) in benzonitrile (4.1×10^{-4} M, 2 mL) containing Et_4NClO_4 (0.1 M) at 1 min intervals.

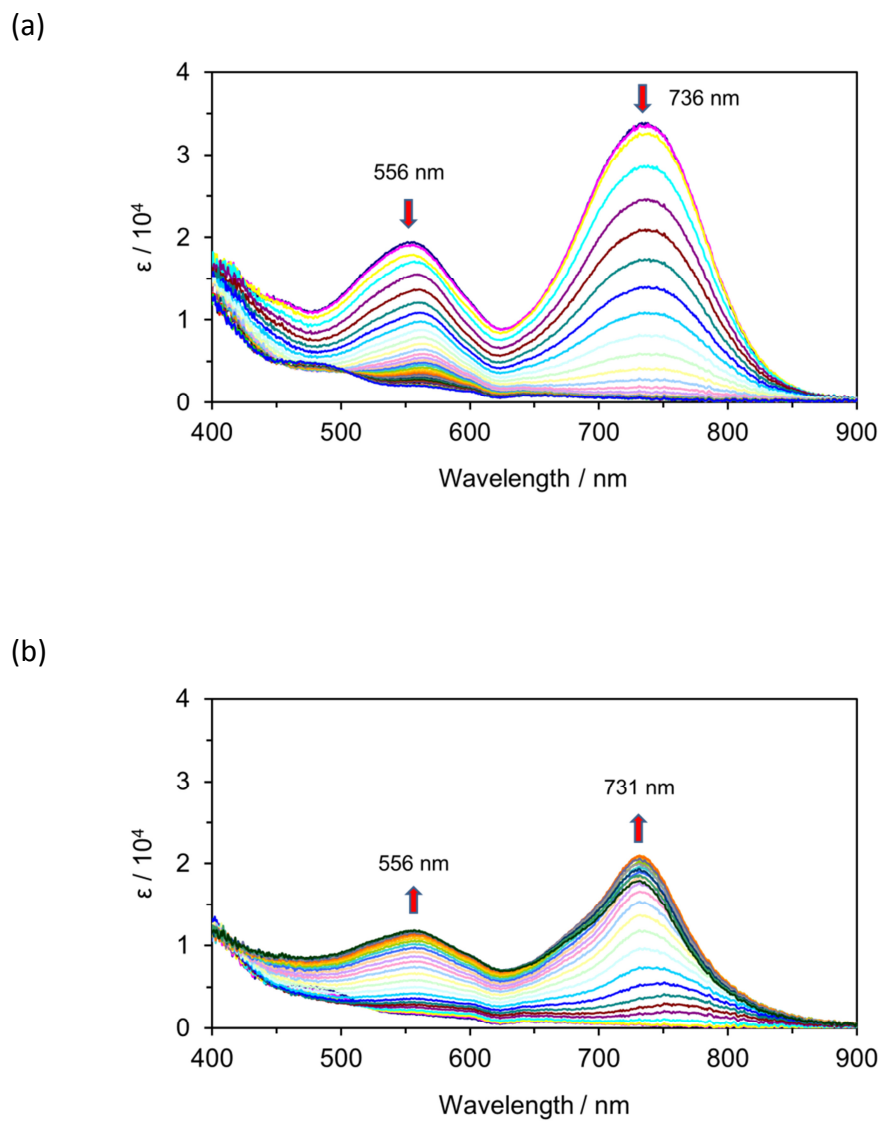


Figure S36. Continuous change in the visible spectrum of $\mathbf{14}^+$: (a) constant-current electrochemical reduction ($70 \mu\text{A}$) and (b) reverse oxidation of the reduced species ($70 \mu\text{A}$) in benzonitrile ($3.9 \times 10^{-4} \text{ M}$, 2 mL) containing Et_4NClO_4 (0.1 M) at 1 min intervals.

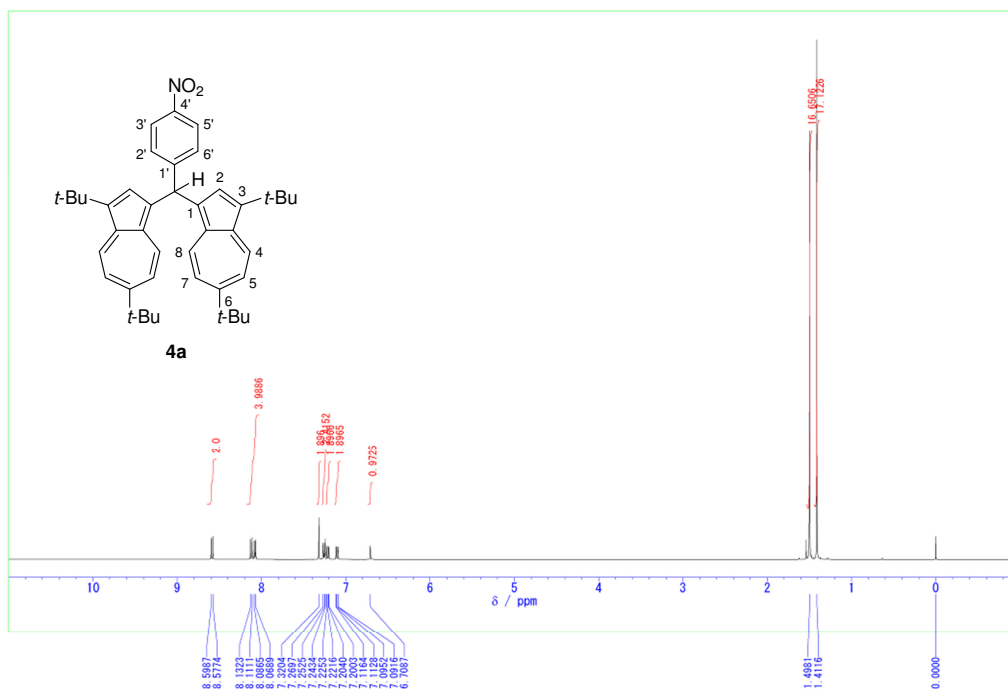
5. Copies of ^1H and ^{13}C NMR spectra of reported compounds

Figure S37. ^1H NMR spectrum (500 MHz) of bis(3,6-di-*tert*-butyl-1-azulenyl)(4-nitrophenyl)methane (**4a**) in CDCl_3 .

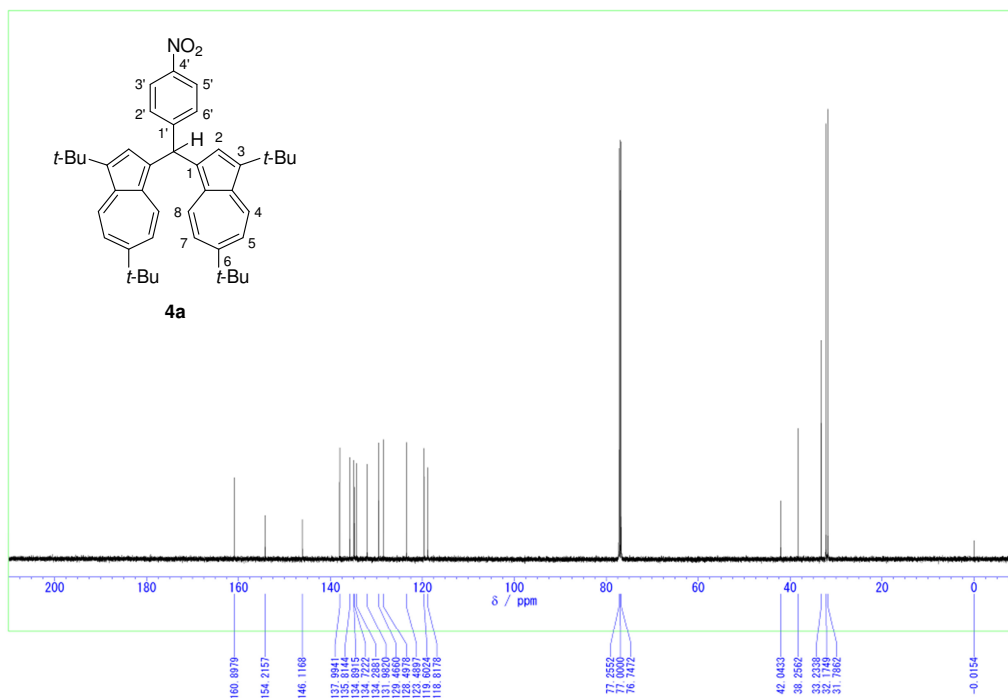


Figure S38. ^{13}C NMR spectrum (125 MHz) of bis(3,6-di-*tert*-butyl-1-azulenyl)(4-nitrophenyl)methane (**4a**) in CDCl_3 .

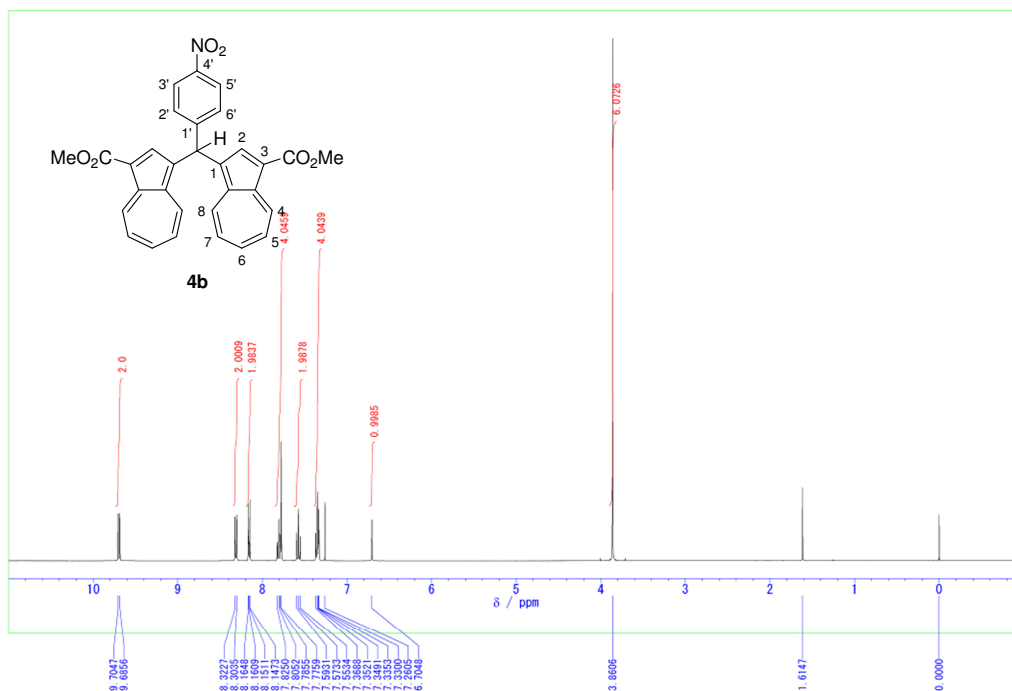


Figure S39. ^1H NMR spectrum (500 MHz) of bis(3-methoxycarbonyl-1-azulenyl)(4-nitrophenyl)methane (**4b**) in CDCl_3 .

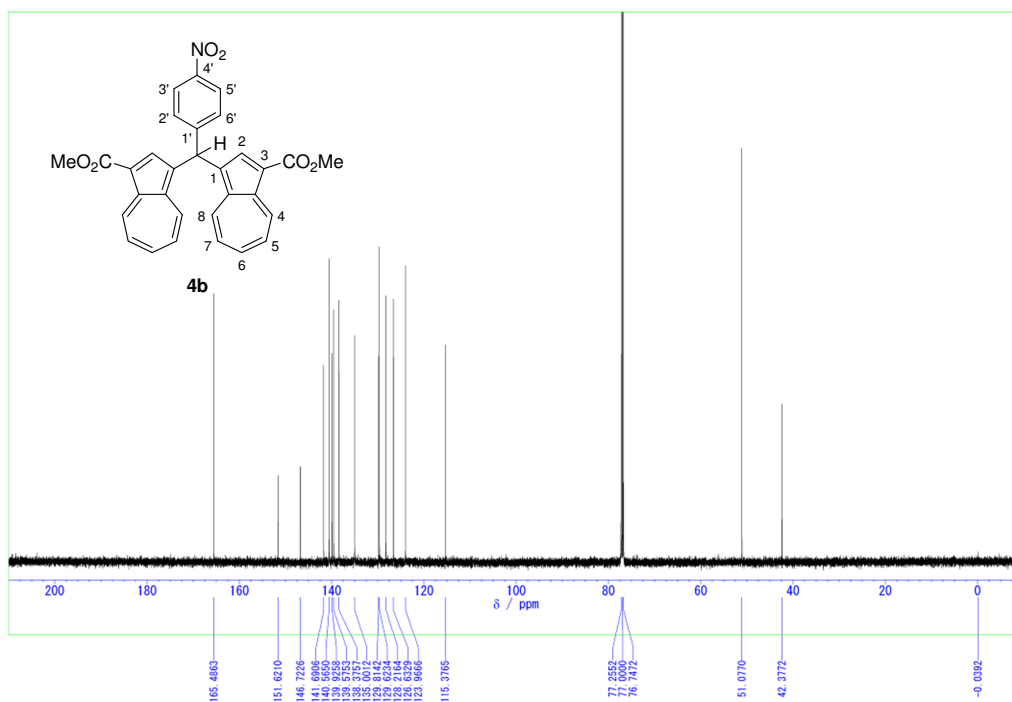


Figure S40. ^{13}C NMR spectrum (125 MHz) of bis(3-methoxycarbonyl-1-azulenyl)(4-nitrophenyl)methane (**4b**) in CDCl_3 .

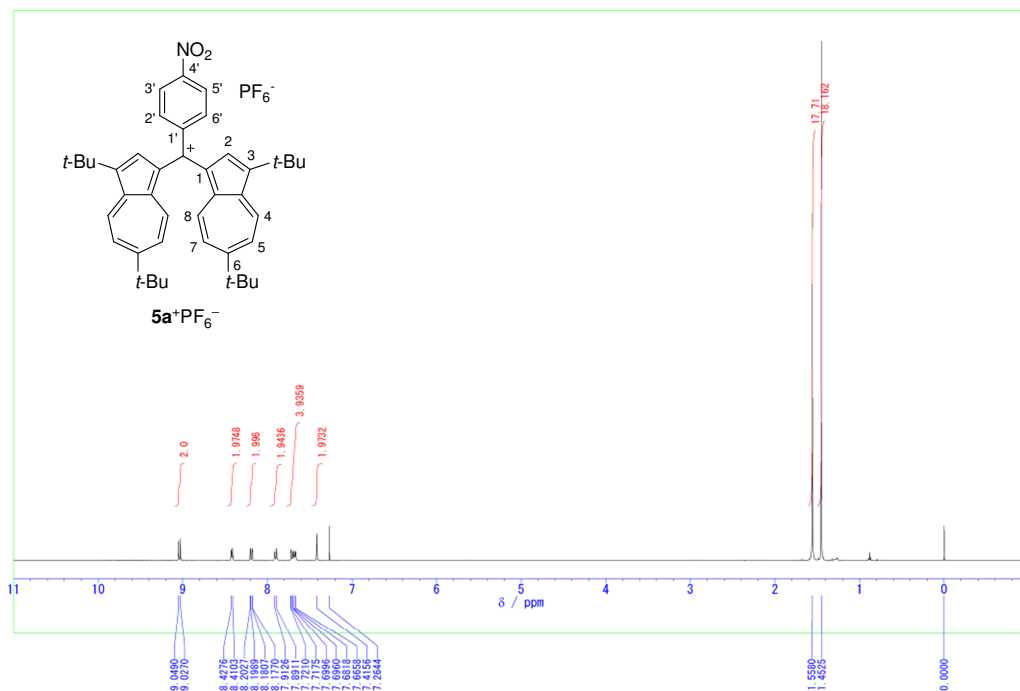


Figure S41. ¹H NMR spectrum (500 MHz) of bis(3,6-di-*tert*-butyl-1-azulenyl)(4-nitrophenyl)methylum hexafluorophosphate (**5a**⁺PF₆⁻) in CDCl₃ at room temperature.

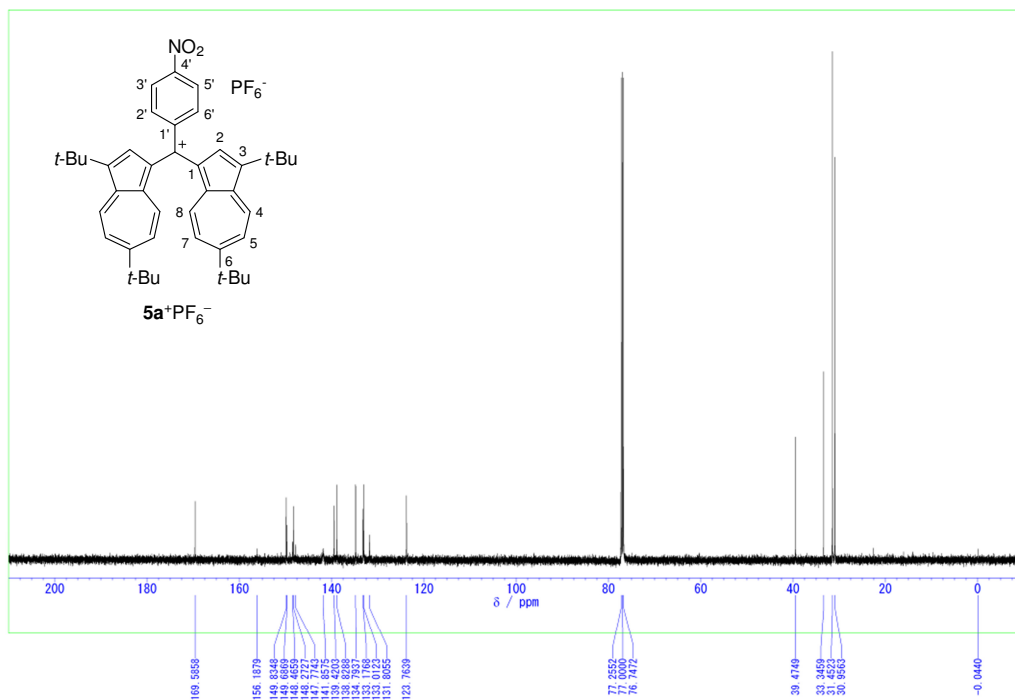


Figure S42. ¹³C NMR spectrum (125 MHz) of bis(3,6-di-*tert*-butyl-1-azulenyl)(4-nitrophenyl)methylum hexafluorophosphate (**5a**⁺PF₆⁻) in CDCl₃ at room temperature.

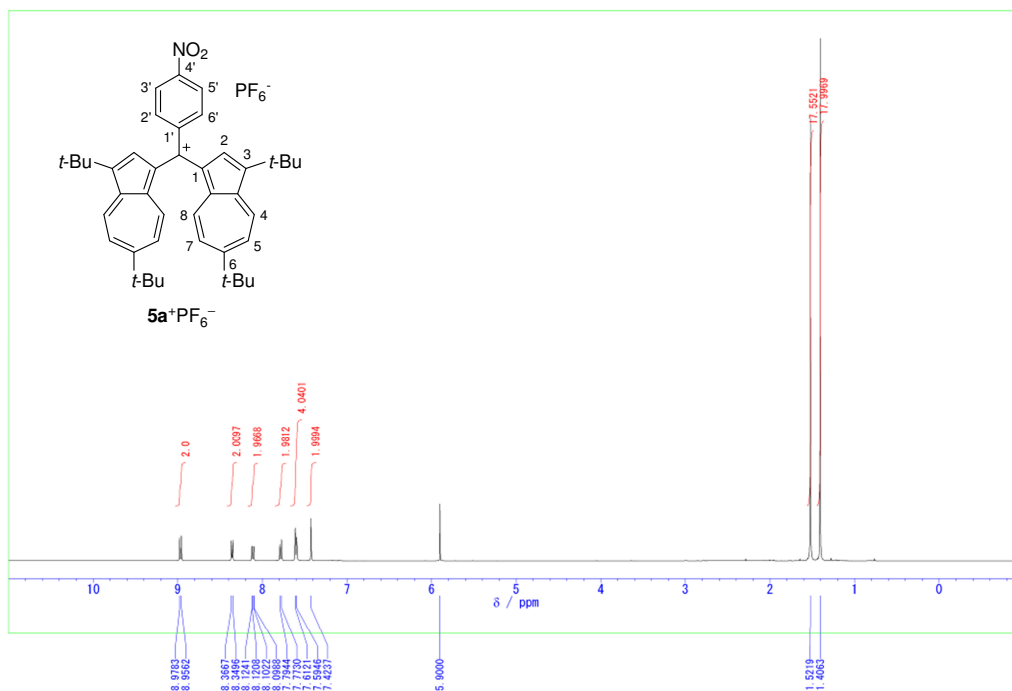


Figure S43. 1H NMR spectrum (500 MHz) of bis(3,6-di-*tert*-butyl-1-azulenyl)(4-nitrophenyl)methylum hexafluorophosphate ($5a^+PF_6^-$) in $(CDCl_2)_2$ at 80 °C.

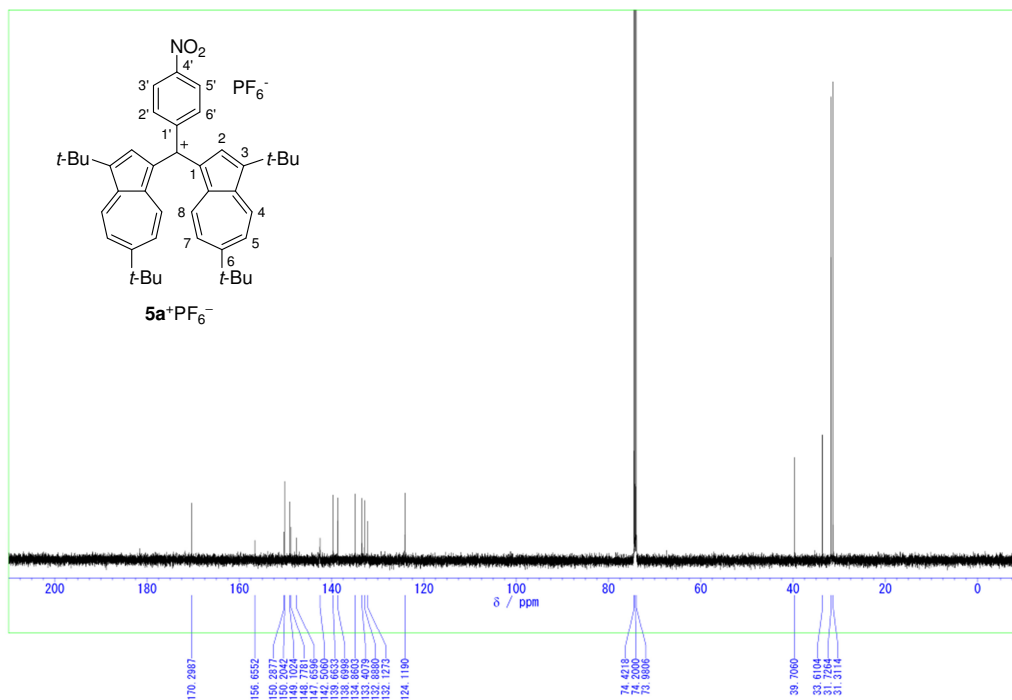


Figure S44. ^{13}C NMR spectrum (125 MHz) of bis(3,6-di-*tert*-butyl-1-azulenyl)(4-nitrophenyl)methylum hexafluorophosphate ($5a^+PF_6^-$) in $(CDCl_2)_2$ at 80 °C.

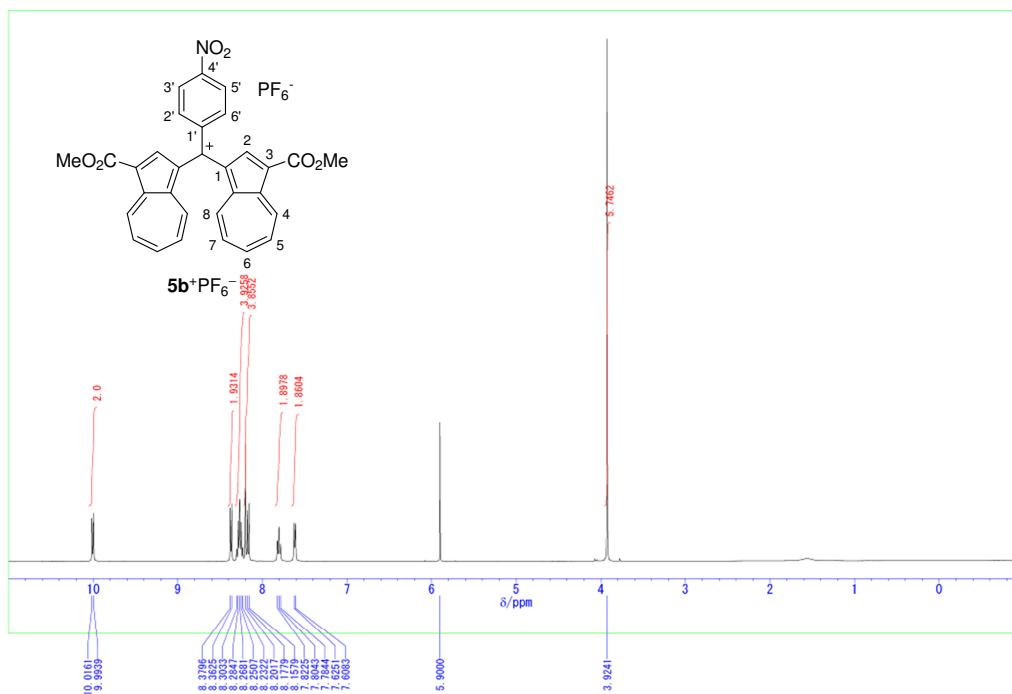
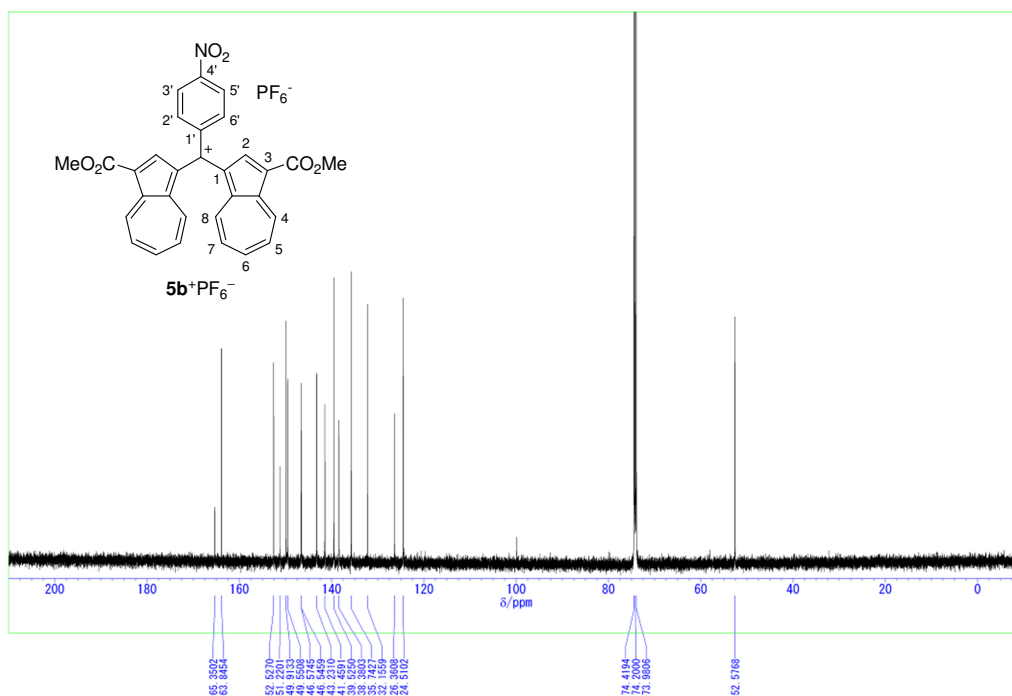


Figure S45. ^1H NMR spectrum (500 MHz) of bis(3-methoxycarbonyl-1-azulenyl)(4-nitrophenyl)methylum hexafluorophosphate ($5b^+\text{PF}_6^-$) in $(\text{CDCl}_2)_2$ at 80°C .



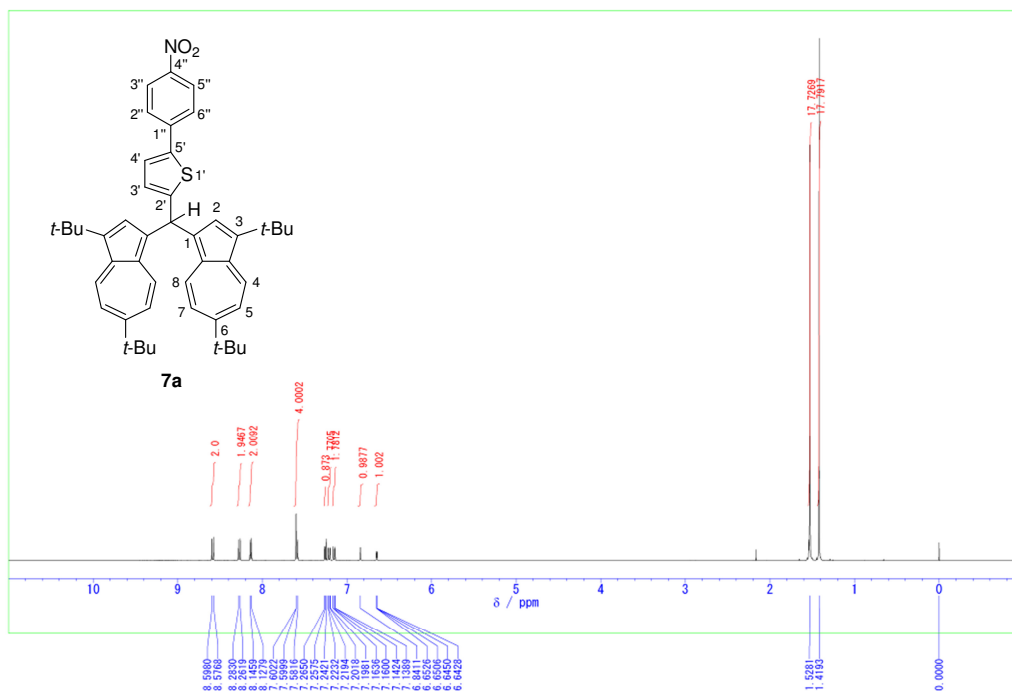


Figure S47. ^1H NMR spectrum (500 MHz) of bis(3,6-di-*tert*-butyl-1-azulenyl)[5-(4-nitrophenyl)-2-thienyl]methane (**7a**) in CDCl_3 .

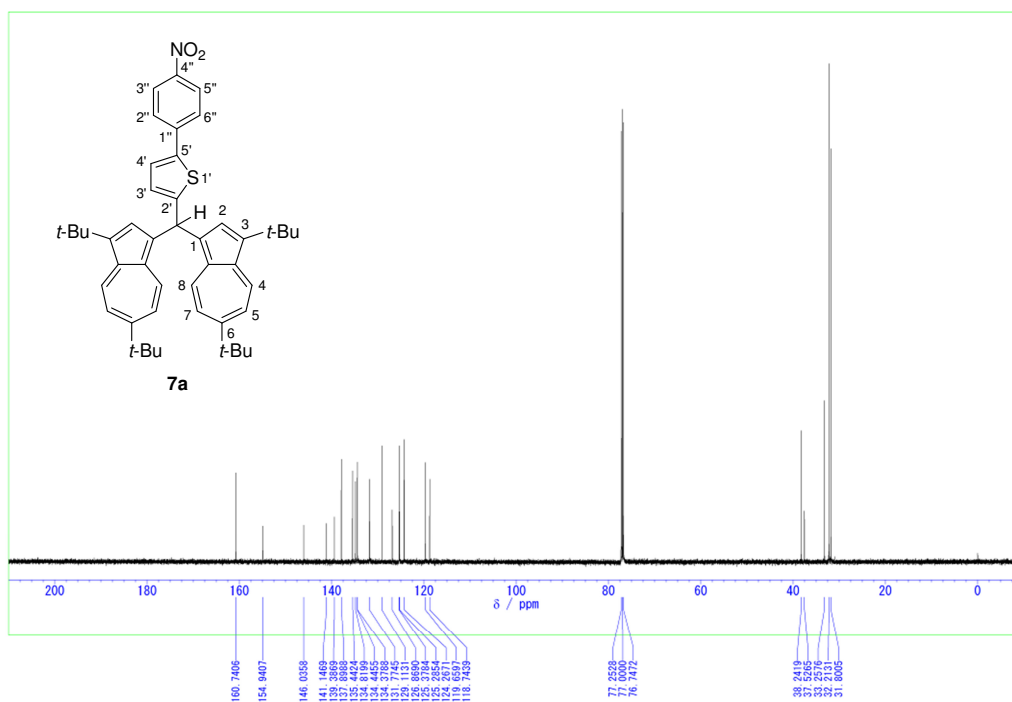


Figure S48. ^{13}C NMR spectrum (125 MHz) of bis(3,6-di-*tert*-butyl-1-azulenyl)[5-(4-nitrophenyl)-2-thienyl]methane (**7a**) in CDCl_3 .

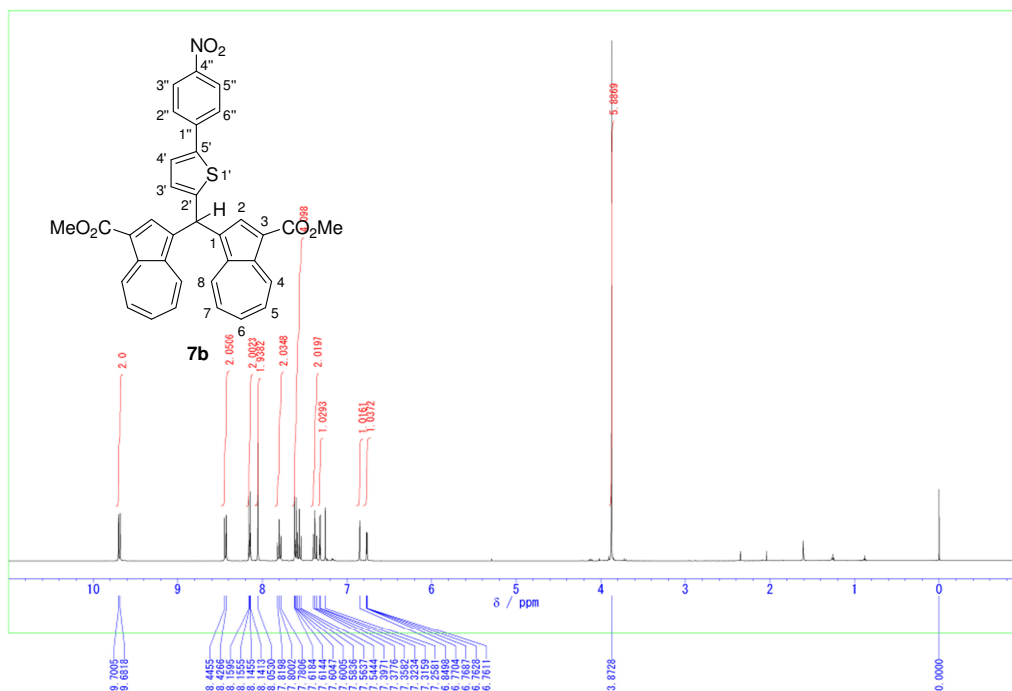
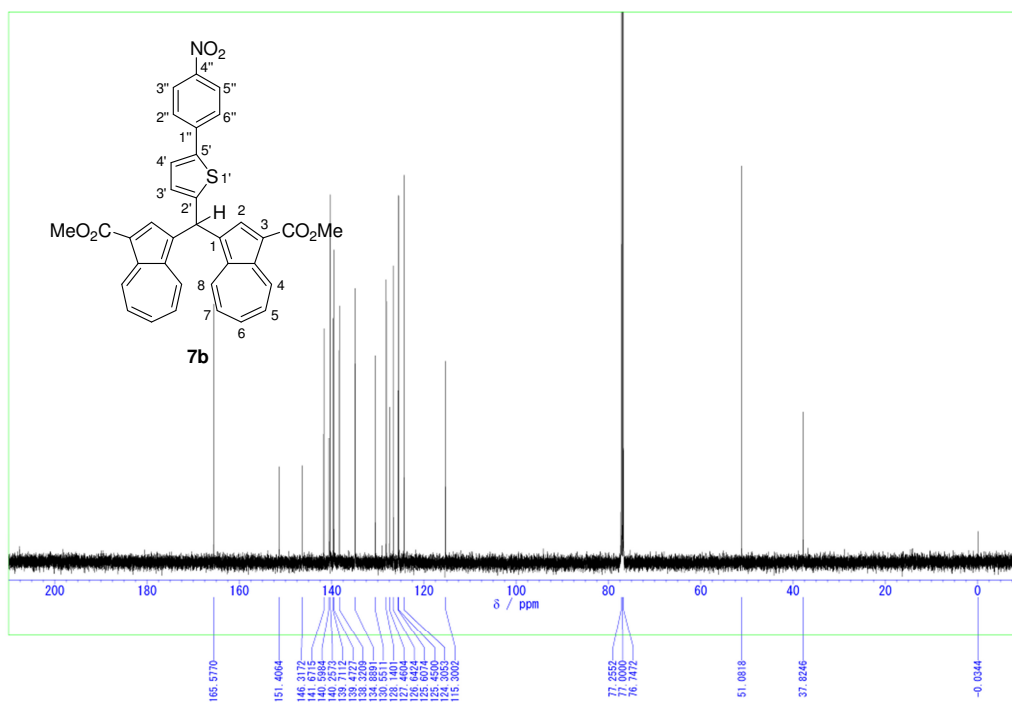


Figure S49. ^1H NMR spectrum (500 MHz) of bis(3-methoxycarbonyl-1-azulenyl)[5-(4-nitrophenyl)-2-thienyl]methane (**7b**) in CDCl_3 .



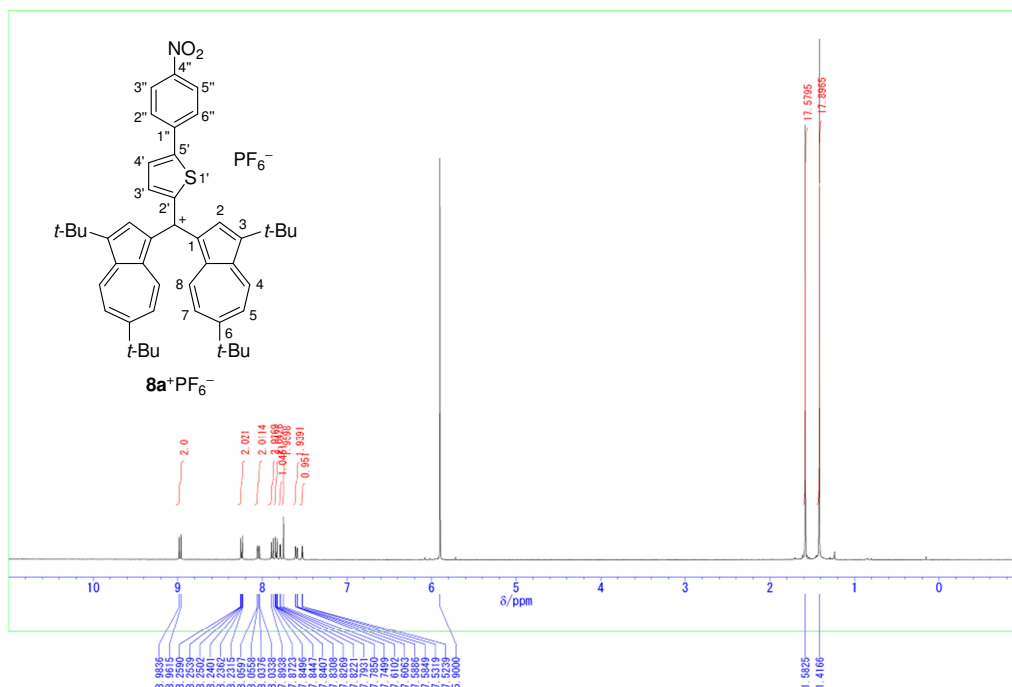


Figure S51. ^1H NMR spectrum (600 MHz) of bis(3,6-di-*tert*-butyl-1-azulenyl)[5-(4-nitrophenyl)-2-thienyl]methylium hexafluorophosphate ($\mathbf{8a}^+\text{PF}_6^-$) in $(\text{CDCl}_2)_2$ at 100°C .

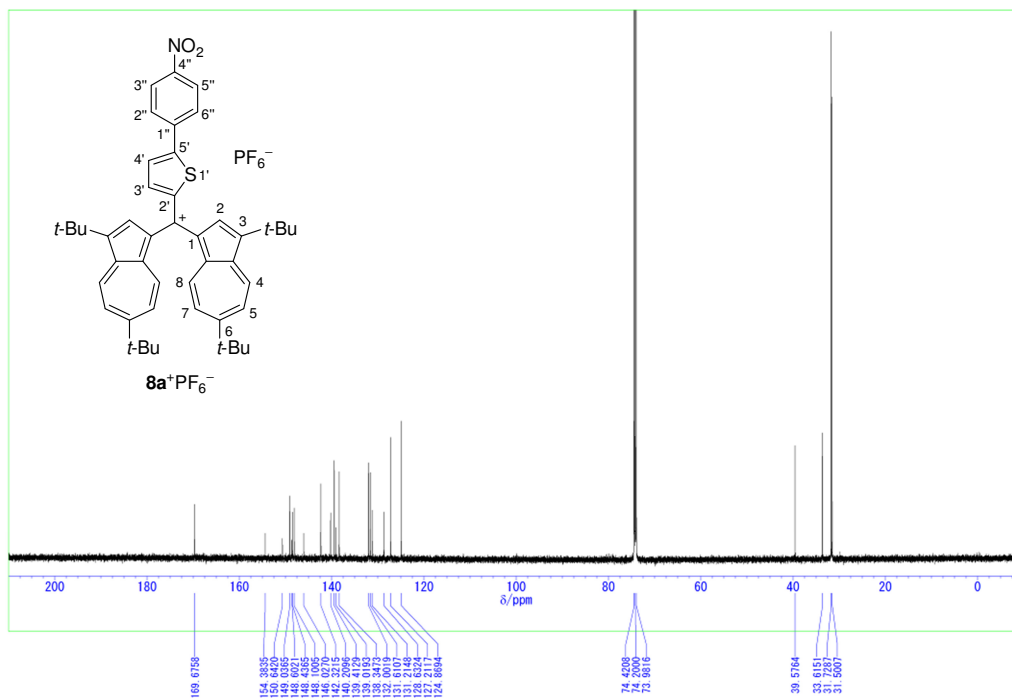


Figure S52. ^{13}C NMR spectrum (150 MHz) of bis(3,6-di-*tert*-butyl-1-azulenyl)[5-(4-nitrophenyl)-2-thienyl]methylium hexafluorophosphate ($\mathbf{8a}^+\text{PF}_6^-$) in $(\text{CDCl}_2)_2$ at 100°C .

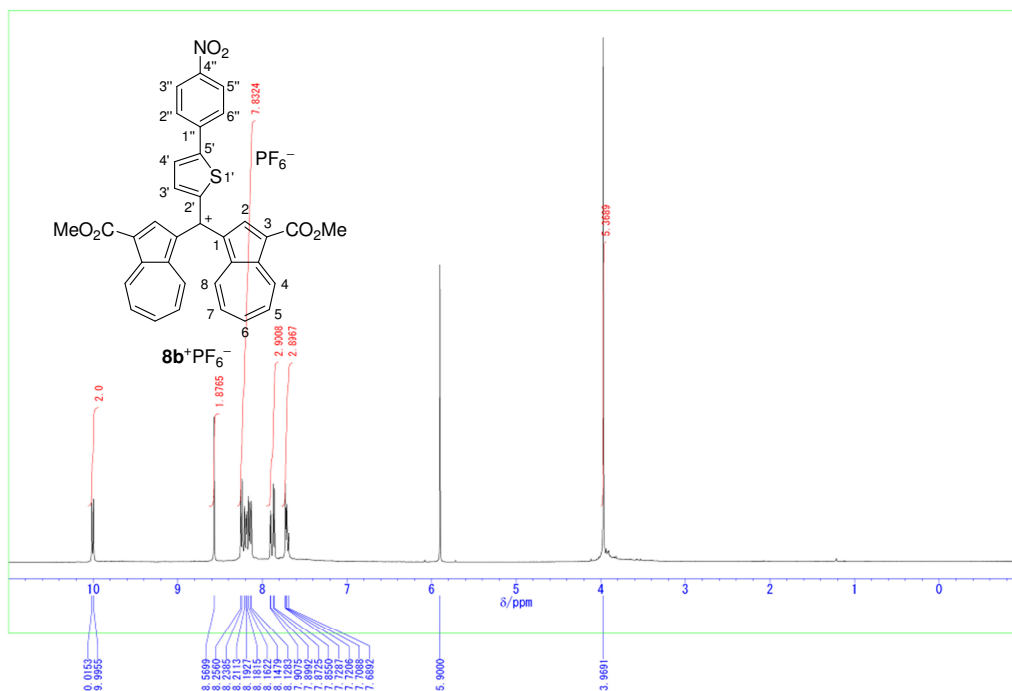


Figure S53. ¹H NMR spectrum (500 MHz) of bis(3-methoxycarbonyl-1-azulenyl)[5-(4-nitrophenyl)-2-thienyl]methylium hexafluorophosphate (**8b**⁺PF₆⁻) in (CDCl₂)₂ at 80 °C.

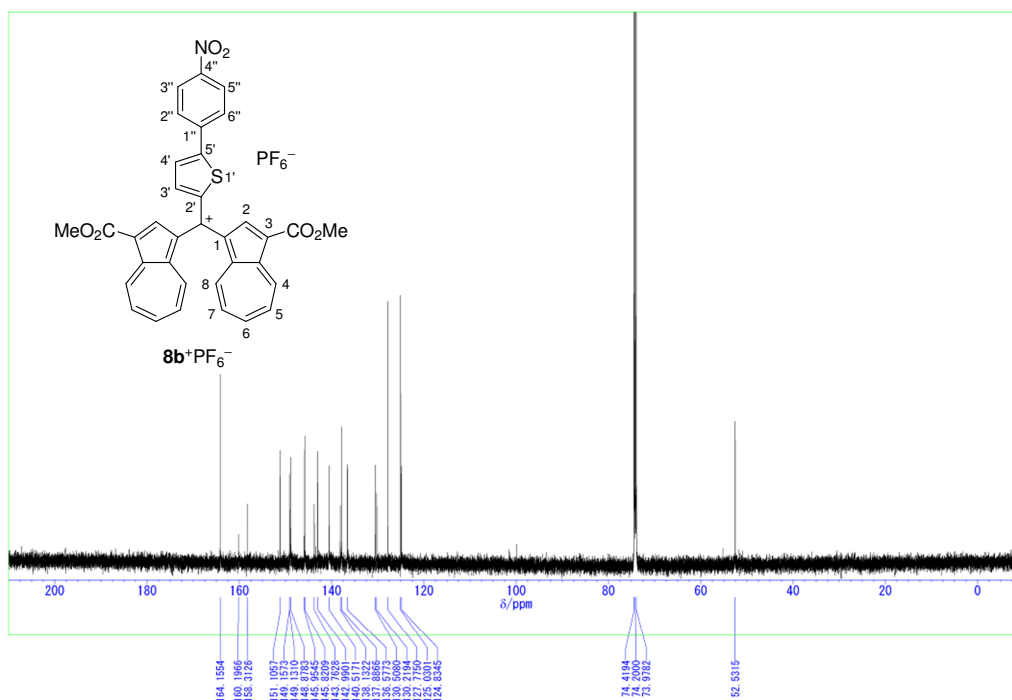


Figure S54. ¹³C NMR spectrum (125 MHz) of bis(3-methoxycarbonyl-1-azulenyl)[5-(4-nitrophenyl)-2-thienyl]methylium hexafluorophosphate (**8b**⁺PF₆⁻) in (CDCl₂)₂ at 80 °C.

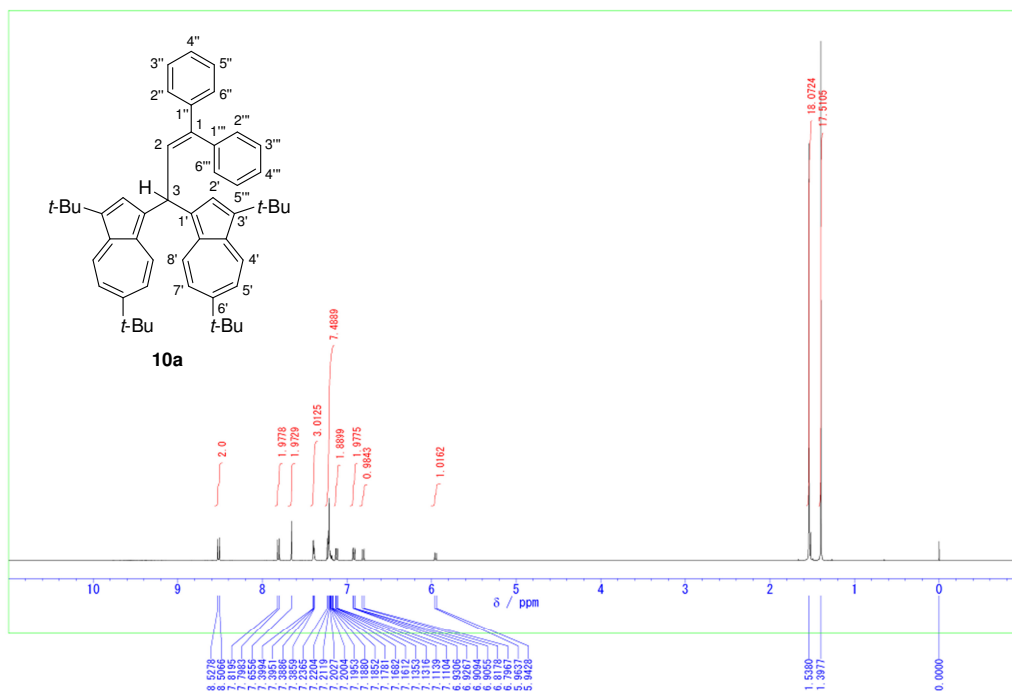


Figure S57. ^1H NMR spectrum (500 MHz) of 3,3-bis(3,6-di-*tert*-butyl-1-azulenyl)-1,1-diphenylpropene (**10a**) in CDCl_3 .

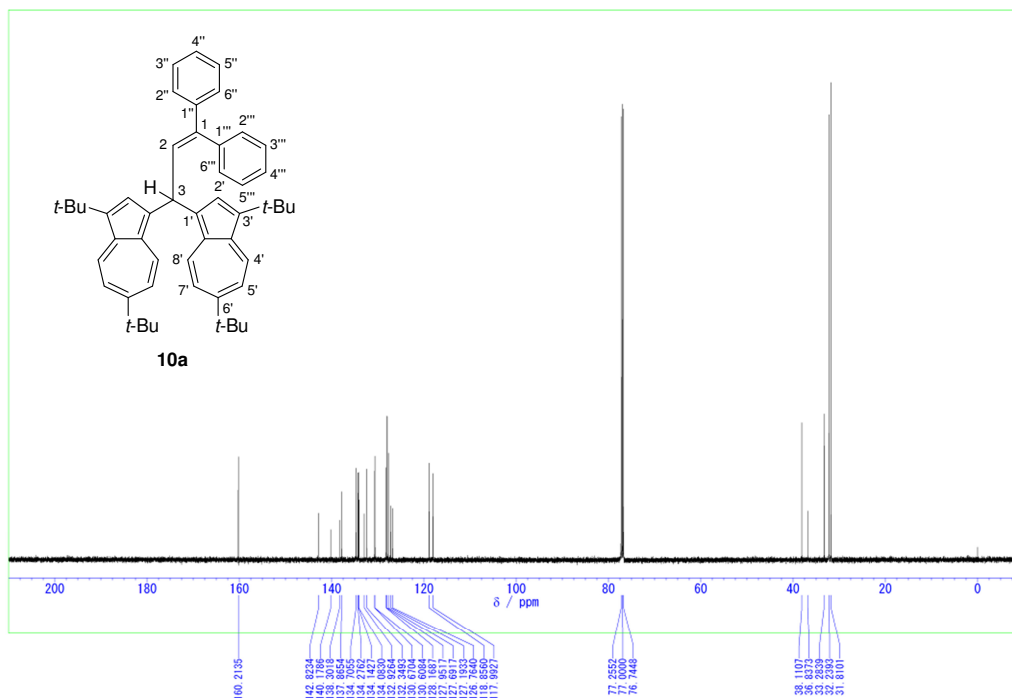


Figure S58. ^{13}C NMR spectrum (125 MHz) of 3,3-bis(3,6-di-*tert*-butyl-1-azulenyl)-1,1-diphenylpropene (**10a**) in CDCl_3 .

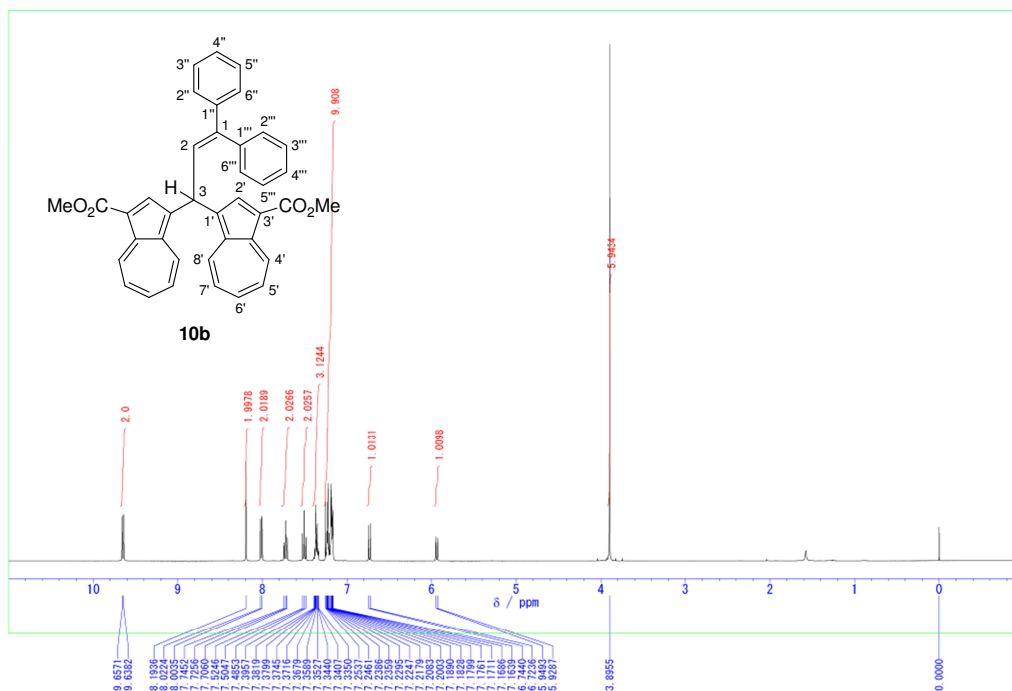


Figure S59. ¹H NMR spectrum (500 MHz) of 3,3-bis(3-methoxycarbonyl-1-azulenyl)-1,1-diphenylpropene (**10b**) in CDCl₃.

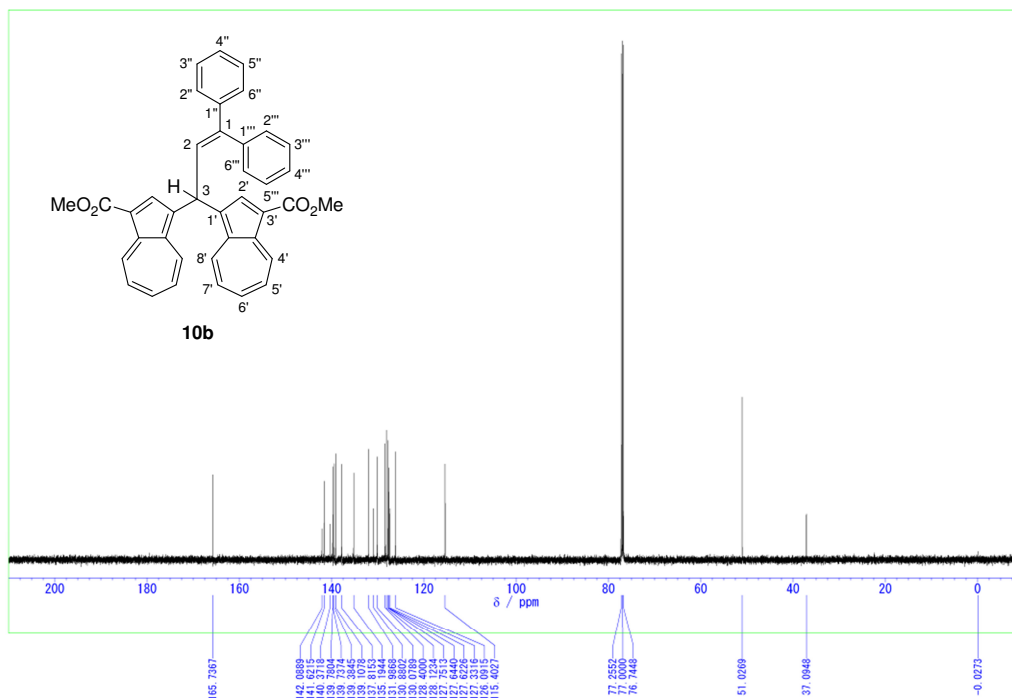


Figure S60. ¹³C NMR spectrum (125 MHz) of 3,3-bis(3-methoxycarbonyl-1-azulenyl)-1,1-diphenylpropene (**10b**) in CDCl₃.

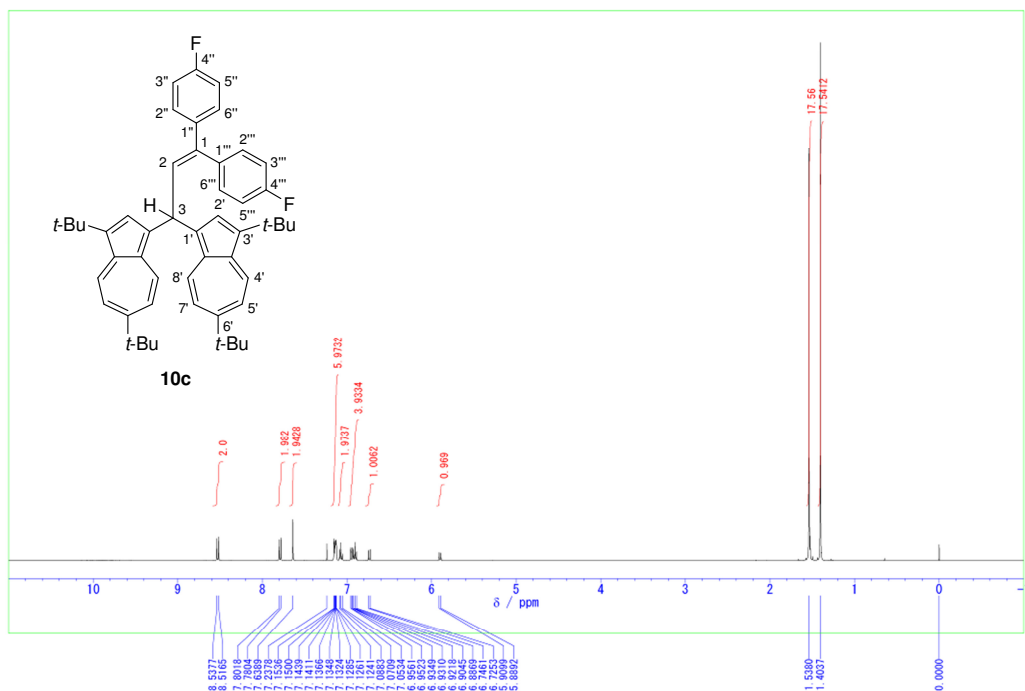


Figure S61. ^1H NMR spectrum (500 MHz) of 3,3-bis(3,6-di-*tert*-butyl-1-azulenyl)-1,1-bis(4-fluorophenyl)propene (**10c**) in CDCl_3 .

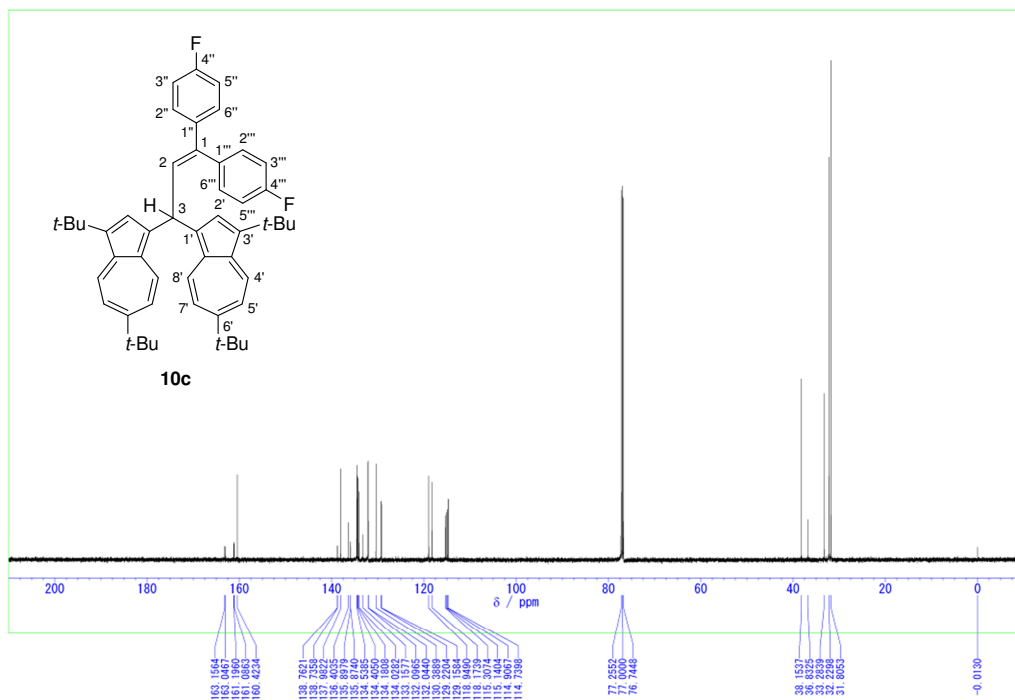


Figure S62. ^{13}C NMR spectrum (125 MHz) of 3,3-bis(3,6-di-*tert*-butyl-1-azulenyl)-1,1-bis(4-fluorophenyl)propene (**10c**) in CDCl_3 .

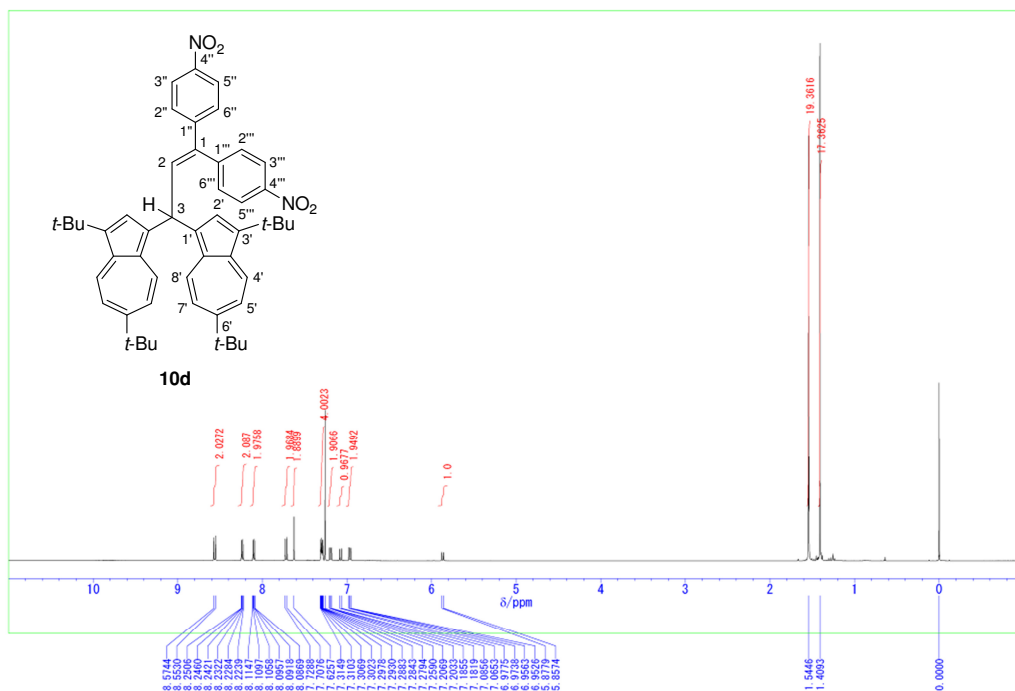


Figure S63. ¹H NMR spectrum (500 MHz) of 3,3-bis(3,6-di-*tert*-butyl-1-azulenyl)-1,1-bis(4-nitrophenyl)propene (**10d**) in CDCl₃.

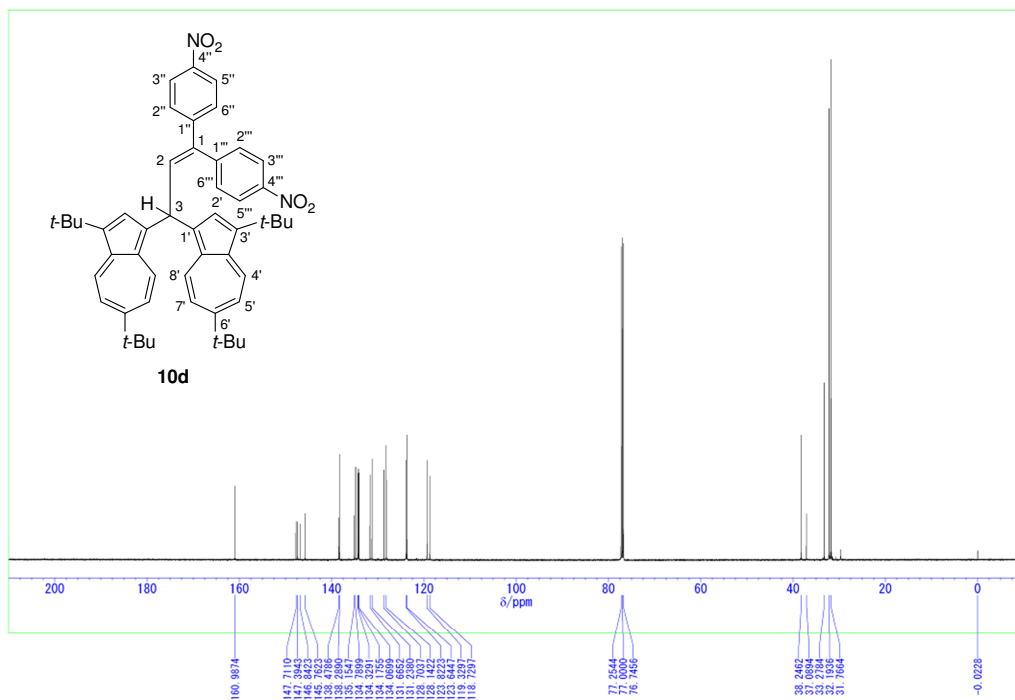


Figure S64. ¹³C NMR spectrum (125 MHz) of 3,3-bis(3,6-di-*tert*-butyl-1-azulenyl)-1,1-bis(4-nitrophenyl)propene (**10d**) in CDCl₃.

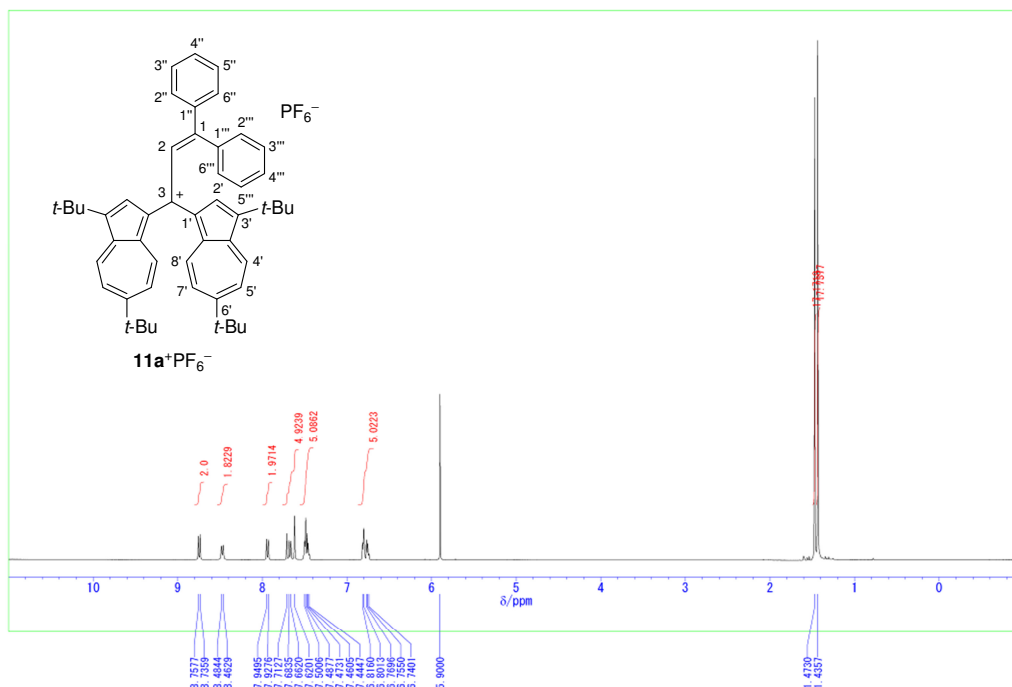


Figure S65. ^1H NMR spectrum (600 MHz) of 3,3-bis(3,6-di-*tert*-butyl-1-azulenyl)-1,1-diphenylpropenylium hexafluorophosphate ($11\text{a}^+\text{PF}_6^-$) in $(\text{CDCl}_2)_2$ at 120°C .

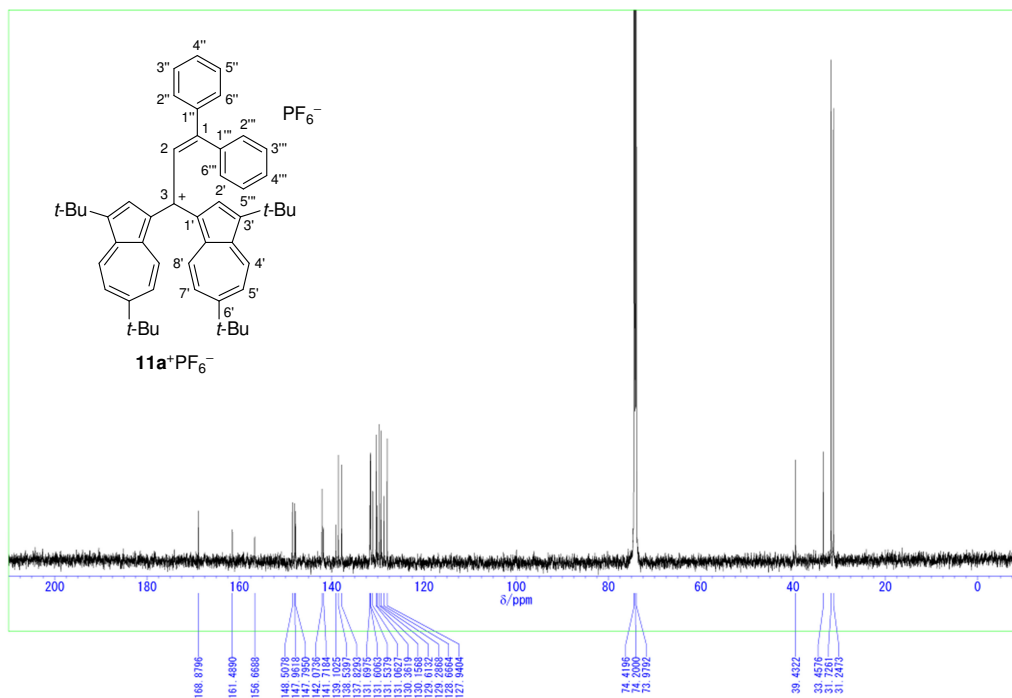


Figure S66. ^{13}C NMR spectrum (150 MHz) of 3,3-bis(3,6-di-*tert*-butyl-1-azulenyl)-1,1-diphenylpropenylium hexafluorophosphate ($11\text{a}^+\text{PF}_6^-$) in $(\text{CDCl}_2)_2$ at 120°C .

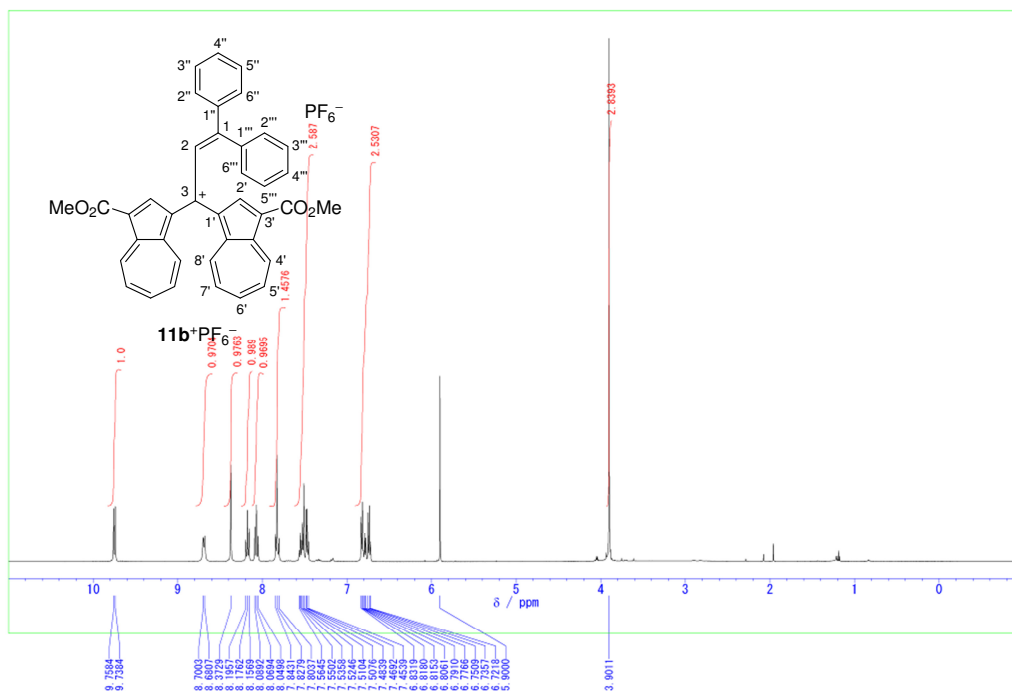


Figure S67. ¹H NMR spectrum (500 MHz) of 3,3-bis(3-methoxycarbonyl-1-azulenyl)-1,1-diphenylpropenylium hexafluorophosphate (**11b**⁺PF₆⁻) in (CDCl₂)₂ at 80 °C.

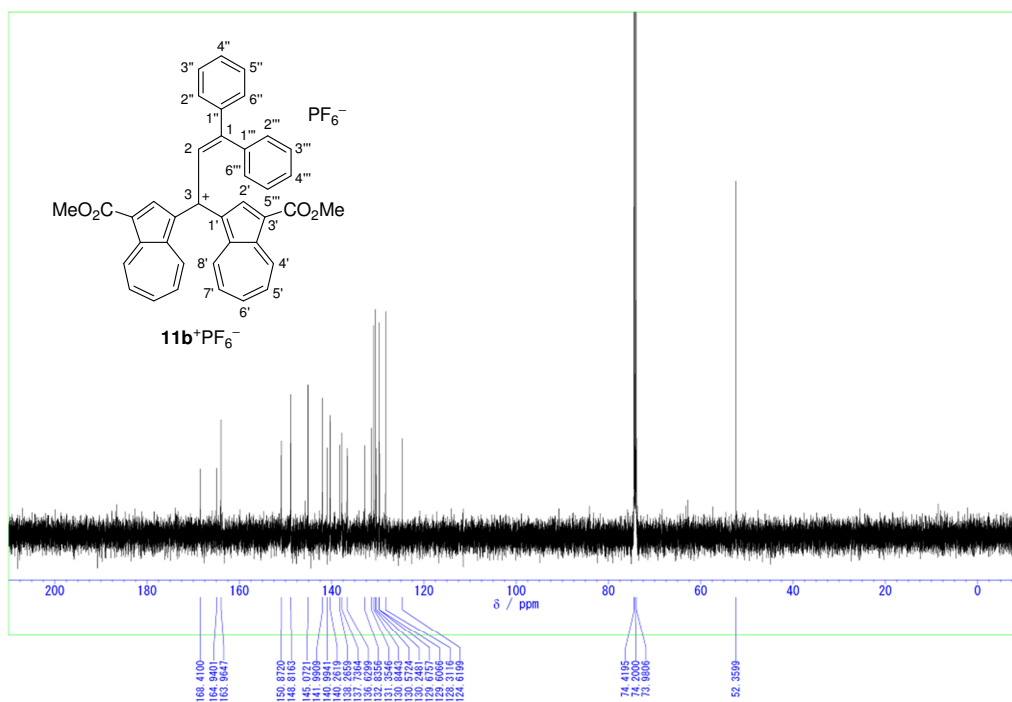


Figure S68. ¹³C NMR spectrum (125 MHz) of 3,3-bis(3-methoxycarbonyl-1-azulenyl)-1,1-diphenylpropenylium hexafluorophosphate (**11b**⁺PF₆⁻) in (CDCl₂)₂ at 80 °C.

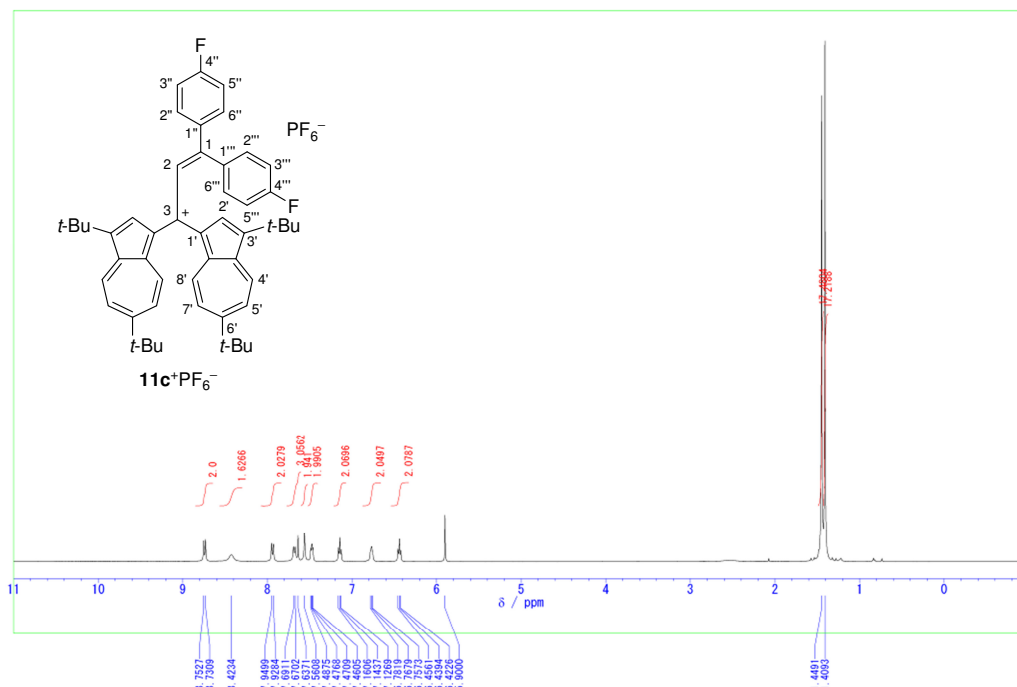


Figure S69. ^1H NMR spectrum (500 MHz) of 3,3-bis(3,6-di-*tert*-butyl-1-azulenyl)-1,1-bis(4-fluorophenyl)propenylium hexafluorophosphate ($11\text{c}^+\text{PF}_6^-$) in $(\text{CDCl}_2)_2$ at 80°C .

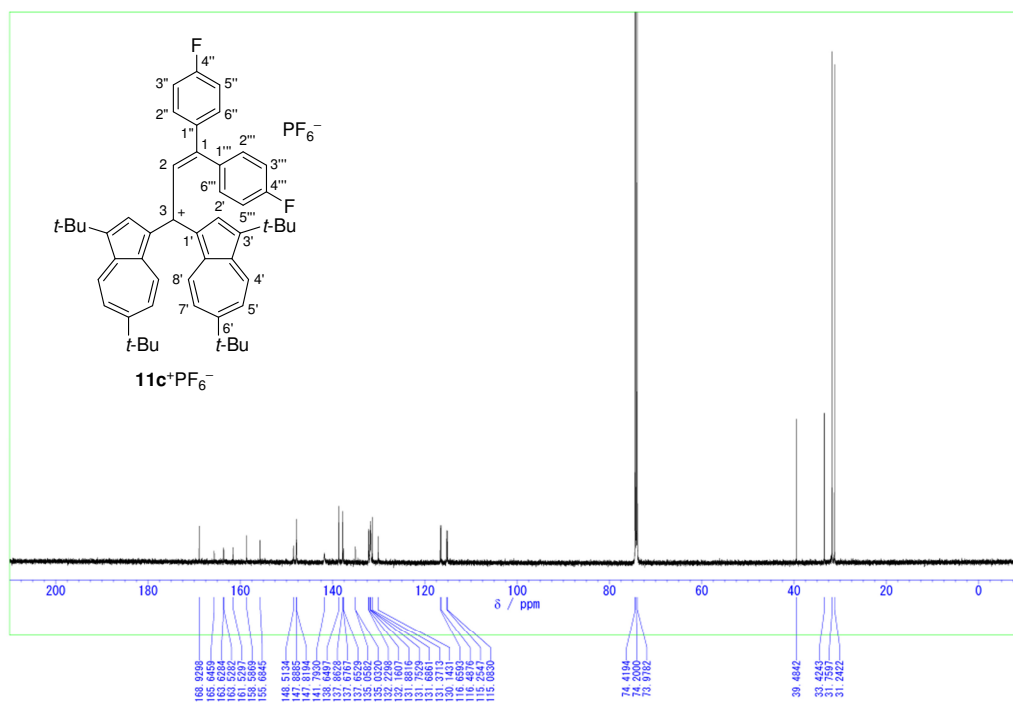


Figure S70. ^{13}C NMR spectrum (125 MHz) of 3,3-bis(3,6-di-*tert*-butyl-1-azulenyl)-1,1-bis(4-fluorophenyl)propenylium hexafluorophosphate ($11\text{c}^+\text{PF}_6^-$) in $(\text{CDCl}_2)_2$ at 80°C .

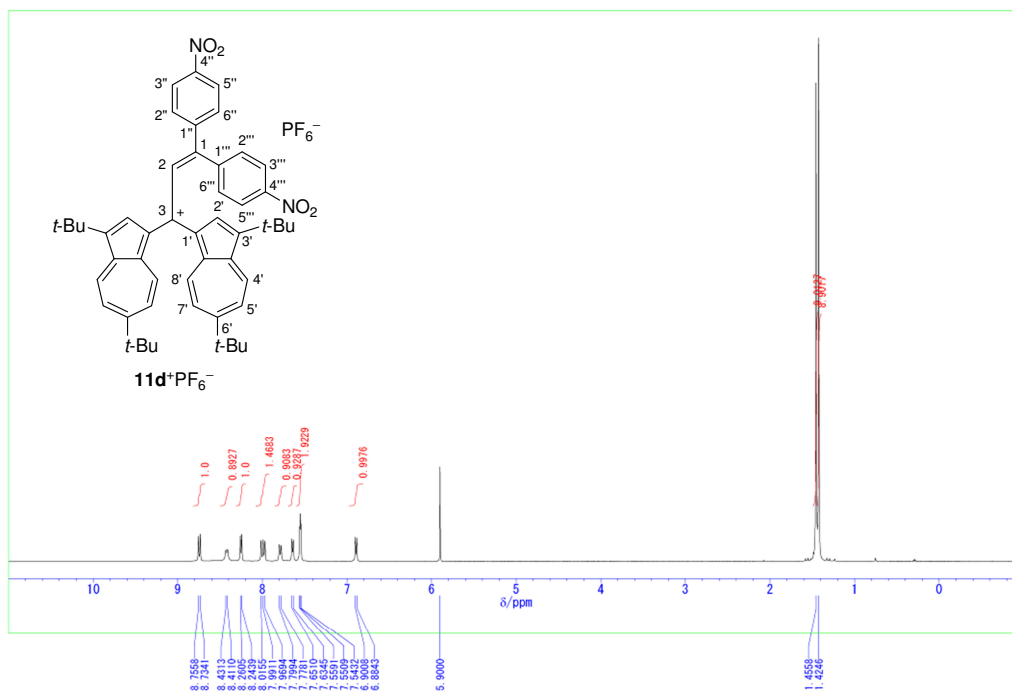
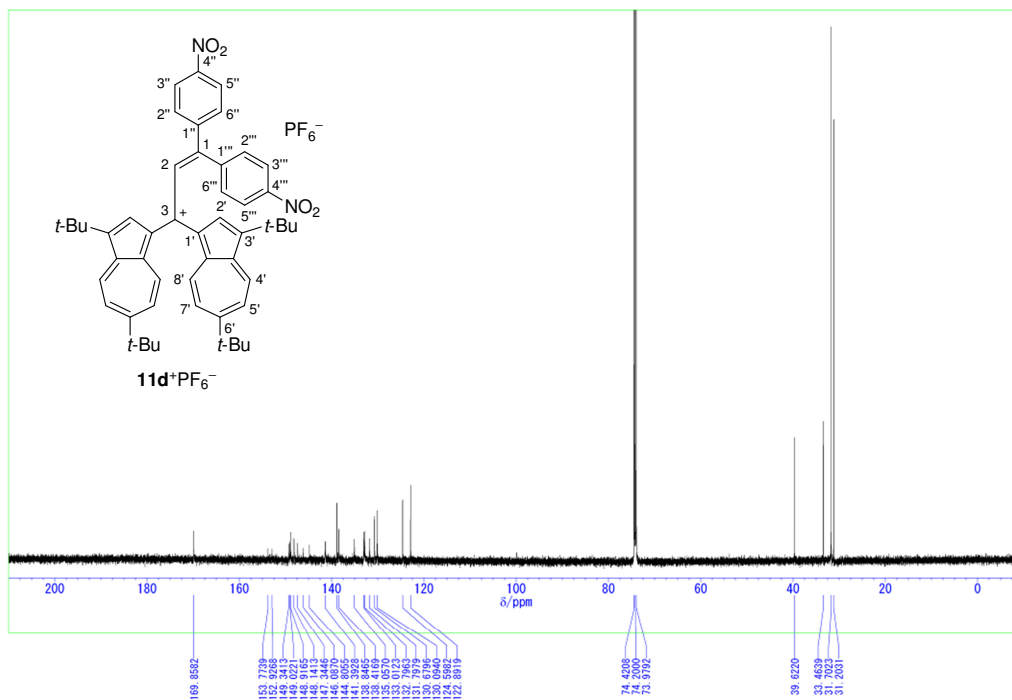


Figure S71. ¹H NMR spectrum (500 MHz) of 3,3-bis(3,6-di-*tert*-butyl-1-azulenyl)-1,1-bis(4-nitrophenyl)propenylium hexafluorophosphate (**11d**⁺PF₆⁻) in CDCl₃.



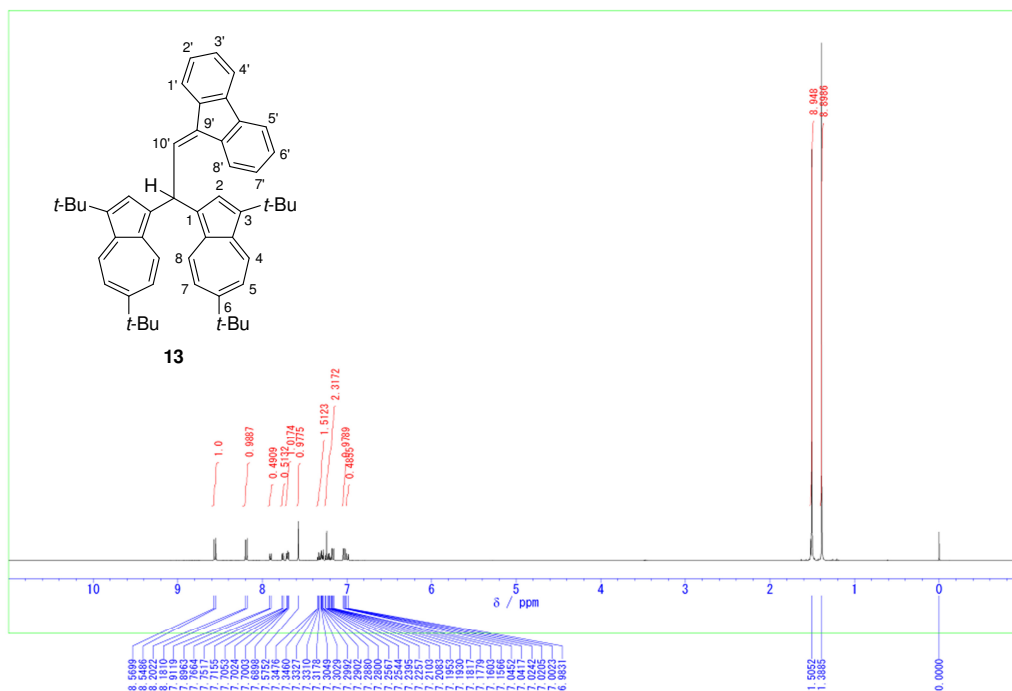


Figure S73. ^1H NMR spectrum (500 MHz) of 9-[2,2-bis(3,6-di-*tert*-butyl-1-azulenyl)ethylidene]-9*H*-fluorene (**13**) in CDCl_3 .

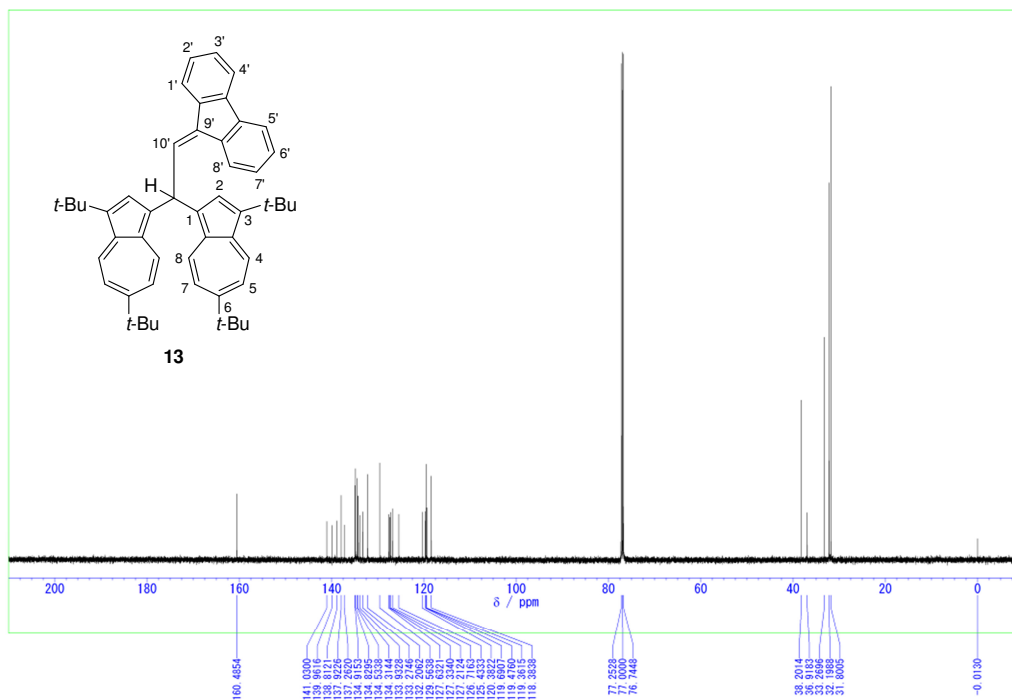


Figure S74. ^{13}C NMR spectrum (125 MHz) of 9-[2,2-bis(3,6-di-*tert*-butyl-1-azulenyl)ethylidene]-9*H*-fluorene (**13**) in CDCl_3 .

